UNIVERSITY OF TWENTE.

Faculty of Electrical Engineering,
Mathematics & Computer Science

Visible Light Positioning for Unmanned Aerial Vehicles

Ricardo Ampudia Hernandez

M.Sc. Thesis
August 2021

TU Delft
Delft University of Technology

4TU.Federation

Supervisors:
Prof. Dr. Paul Havinga
Dr. Ir. Yanqiu Huang
Dr. Marco Zuñiga

Faculty of Electrical Engineering,
Mathematics and Computer Science
University of Twente
P.O. Box 217
7500 AE Enschede
The Netherlands

ABSTRACT

Visible light communication (VLC) is a wireless technology that has gained wide interest in industry and academia due to its ability to achieve power efficient wireless communication at high data rates. With the use of LEDs, VLC can take advantage of the existing lighting infrastructure, and relieve some of the traffic requirements of the increasingly saturated radio-frequency (RF) spectrum. One attractive use case of VLC is for indoor positioning, where the directional characteristics of light allows to achieve centimeter-level accuracy, an impractical challenge for other technologies such as WiFi and Bluetooth. Many applications in industry require accurate and private indoor positioning, such as asset management and tracking. In particular, the use of unmanned aerial vehicles (UAVs) has recently gained interest for related applications involving warehouse management, but requires precise localization that can be expensive to achieve with RF technologies. Visible light positioning (VLP) offers great potential for industrial applications involving UAVs due to its power efficiency and high accuracy, but the topic remains largely unexplored.

In this master thesis, we first provide a thorough analysis of state-of-the-art VLP methods, and identify the best alternatives considering the energy, processing, and design limitations of a constrained drone environment. Then, we propose the use of standard light bulbs to provide localization for drones. We modulate the intensity of the LED sources to send beacons that can be decoded with a simple photodiode in the drone. This optical information is combined with the inertial and altitude sensors in the drones to provide localization without the need for radio, GPS, or cameras. Our framework is the first to provide 3D drone localization with light and we evaluate it with a testbed consisting of four light transmitters and a mini-drone. We show that the proposed approach allows to locate the drone within a few decimeters of the actual position, and reduces the localization error by 42% compared to state-of-the-art positioning methods.

PREFACE

This thesis concludes my research work at Delft University of Technology and my Master program in Embedded Systems at the University of Twente. This experience that started in 2019 has been more challenging and amusing than I could have expected at the beginning, which makes the completion of this stage very meaningful.

I would like to thank my supervisors, whose feedback and guidance were critical to complete my thesis. First, I want to express my gratitude to Marco Zuñiga, who accepted me as part of the Embedded and Networked Systems group at TU Delft. After countless meetings, he got through my stubborn head and made me realize that research starts where engineering ends; and that ideas are more valuable when communicated effectively. A special thank you to Yanqiu Huang, whose kind feedback helped me not only improve, but also to appreciate my work in periods of doubt. I want to acknowledge the contribution of Talia Xu, who was thorough when reviewing this work and immensely helped me to consolidate my research. I would also like to thank Paul Havinga for being part of the graduation committee.

Finally, I want to use this space to show my appreciation to the people who were an important part of my master's experience, even before it began. To my grandfather, who has always been an inspiration to pursue a technical career. To Carlos Tapia, who encouraged me to go after this adventure. Thank you to my friends Sara, Valeria and Arnaud, we survived the Netherlands together. Last but not least, I would like to thank my parents and sister for their continuous love and support.

Ricardo Ampudia
Delft, The Netherlands
August 19th, 2021

CONTENTS

LIST OF ACRONYMS

ADC	Analog-to-Digital Converter
ADOA	Angle Difference of Arrival
AOA	Angle Of Arrival
CCW	Counter Clockwise
CDM	Code Division Multiplexing
CW	Clockwise
DoF	Degrees of Freedom
ENU	East North Up
FDM	Frequency Divison Multiplexing
FDMA	Frequency-Division Multiple Access
FFT	Fast Fourier Transform
FOV	Field Of View
GA	Genetic Algorithm
GPS	Global Positioning System
IMU	Inertial Measurement Unit
LED	Light-Emitting Diode
LOS	Line of Sight
PCB	Printed Circuit Board
PD	Photodiode
PSO	Particle Swarm Optimization
RF	Radio Frequency
RSS	Received Signal Strength
Rx	Receiver
SoA	State-of-the-Art
TDM	Time Division Multiplexing
TOA	Time of Arrival

Tx Transmitter

UAV Unmanned Aerial Vehicle

UWB Ultra Wide Band

VLC Visible Light Communication

VLP Visible Light Positioning

List of Figures

List of Tables

1 INTRODUCTION

As a result of a large number of mobile devices capable of wireless communication, the use of radio-frequency (RF) based technologies has presented many challenges due to an increased saturation in the electromagnetic spectrum. In the last two decades, the large amount of smart devices requiring connectivity has resulted in an insufficient capacity of the current infrastructure to meet the traffic requirements. In parallel, the advancements in solid-state electronics have enabled the achievement of high luminescence LEDs that are efficient in terms of power consumption when compared to incandescent bulbs. In combination, these two events have been a driving force for a growing trend in research called visible light communication (VLC) that extends the possibilities for wireless communications [1].

VLC is a technology that exploits the fast switching capabilities of LEDs to transmit encoded data at a rate that is imperceptible to the human eye. VLC is a cost-effective solution that utilizes the existing lighting infrastructure for communication and illumination simultaneously. In addition, the frequency band of VLC is thousands of times larger than radio, which allows to achieve data rates up to multiple Gbps [2]. These and more characteristics, make VLC a viable alternative for wireless communication that can be complementary to the use of WiFi and cellular data.

The use of VLC for indoor location services is one application that has captured the enthusiasm of researchers due to its ability to achieve sub-meter accuracy. The directional characteristics of light make it less susceptible than RF waves to multipath propagation effects, which improves the reliability of measurements used for localization [3]. With the use of low cost, flexible and energy efficient LEDs and Photodiodes (PDs), visible light positioning (VLP) provides considerable advantages compared to WiFi, Bluetooth and ultra-wideband (UWB) which achieve at best, the same positioning accuracy at a much higher cost [4]. For the previous reasons, the use of VLP has gained interest in industry for several applications involving warehousing, asset management and manufacturing [5] as it does not raise the privacy concerns of cameras.

Another important trend in industry is the use of unmanned aerial vehicles (UAVs) as a solution for some of the applications mentioned above. For example, utilizing drones as an alternative to perform visual inspections in areas that are difficult to reach or possibly unsafe for workers e.g. manufacturing environments and nuclear power plants. An additional use case of interest is for autonomous inventory management, where information can be collected by drones reading tags or barcodes across a warehouse [6]. Some companies like Eyesee and DroneScan already provide warehousing services using flying robots [7, 8].

Despite the interest of the industry for both VLP and UAVs, their combined use is still largely unexplored and offers great potential for research. The use of VLP enables the possibility to provide accurate indoor positioning with a minimal cost of infrastructure due to the availability of LEDs used for illumination. In addition, the use of low power LEDs and PDs is a suitable choice for communication and positioning in battery constrained devices such as UAVs.

1.1 Problem statement

There are several limitations in the available technologies when considering localization for UAVs. The problem of outdoor positioning for drones has been mostly solved with the use of GPS. However, for indoor spaces where GPS fails to meet good levels of performance, alternatives solutions are required. Some technologies, like UWB and cameras, are able to provide indoor positioning services but require expensive infrastructure to work. In addition, cameras raise privacy concerns that make them undesirable and even restricted in certain areas [9]. Other options, like WiFi and Bluetooth, can leverage many existing access points and devices but do not provide reliable nor accurate performance. In contrast, VLP offers a promising alternative for accurate localization that takes advantage of the lighting already available in closed spaces.

While a substantial number of VLP methods are available in the state-of-the-art (SoA), some require complex infrastructure arrangements which are not suitable for UAVs when considering their energy, weight and processing constraints. In addition, most of the literature centers on testing for static scenarios where a receiver is fixed [4], which does not reflect the reality of drones who are exposed to rapid movement and rotations. Currently, *there is no identified VLP framework that considers simple infrastructure requirements and that takes into account the mobility of a UAV application*.

1.2 Research goal and contributions

The motivation of this project is based on the interest for VLP in research and its use for several industrial applications, including UAVs. In addition, due to the lack of available VLP methods that consider the mobile scenarios encountered by drones, the goal of this master thesis is to:

Achieve 3D indoor localization for unmanned aerial vehicles with visible light positioning.

Aligned to the project goal, the main contributions of this thesis are summarized as follows:

- *Contribution 1: SoA analysis. [Chapter 3]* Considering that the state-of-the-art already provides notable contributions on visible light positioning [4, 10, 11], we perform a thorough analysis of the existing methods and show that the approach decomposing the 3D positioning problem into a 2D+H problem (where H stands for height) is the best alternative for UAVs [12, 13].
- *Contribution 2: A novel framework, Firefly, for UAV localization. [Chapter 4]* We identify the limitations of the 2D+H approach on drones, due to the high number of degrees of freedom (DoF), and propose the Firefly framework. Firefly combines visible light information, together with the inertial and altitude sensors in drones, to attain accurate 3D localization. A key property of our framework is the low complexity of the HW (transmitters and receiver) and SW (localization method).
- *Contribution 3: First experimental evaluation with 6 DoF. [Chapter 5 & Chapter 6].* We build a testbed using a real drone and evaluate VLP methods in an experimental setup that involves movement and rotations for the first time. The testbed works in the dark as well as in scenarios exposed to ambient light. Our main result shows that the localization of drones can be improved by 42% compared to available methods in the state-of-the-art.

1.3 Structure

In Chapter 2, we give the necessary background in VLC, VLP, and localization algorithms that serve as a basis for our work. The contributions listed above are then covered in chapters 3 to 6, as indicated in Section 1.2 . Finally, we present in Chapter 7 the conclusion for future work in this project.

2 BACKGROUND

In this Chapter, we cover the basic concepts of visible light communication and the framework of equations that are used in most VLP methods. We also describe the working principle of common localization algorithms and multiplexing schemes, which serve as a basis to better understand the analysis of the SoA and our own method in the following chapters. We finally mention some of the challenges that can be expected when attempting VLP in the context of UAVs.

2.1 Visible Light Communication

Visible Light Communication is an emerging technology for wireless communication that is expected to become relevant for daily use in the near future. Due to its capacity to achieve data rates up to multiple Gbps with a low power consumption, it is a viable alternative to provide connectivity for a number of devices. In addition, radio-frequency communication, which is usually used in wireless technologies such as WiFi, 4G and Bluetooth, has faced limitations in the last decade to meet the traffic requirements of an increasing amount of *smart* devices. To solve this problem, VLC offers complementary benefits to RF communication. First, it has hundreds of terahertz available in the spectrum (see figure 2.1) which are currently license-free [1]. Second, illumination is expected to consist almost entirely of LEDs for general services by the year 2030 [14], which will make VLC a cost-effective solution to support network connections. Finally, the use of VLC can also provide secure cells for communications which improve privacy in local area networks, making it harder to eavesdrop since this would require a direct line-of-sight (LOS) with the victim.

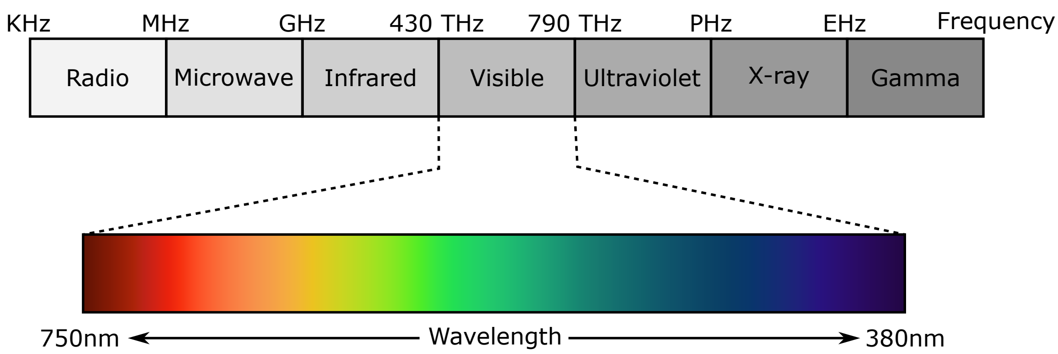

Figure 2.1: Visible light spectrum within the complete electromagnetic spectrum.

While visible light communication offers a great number of advantages, it also presents technical challenges that have yet to be overcome. Due to the directional characteristic of light, obstructions or small changes in orientation can greatly affect the transmitting capacity of the link. This means that in environments with multiple objects and mobile receivers, establishing reliable VLC can be problematic due to occasional blocking and tilting. Other important issues in VLC research include the problem of achieving longer distance range for communication and reducing the sensitivity to ambient light noise.

2.2 Visible Light Positioning

The use of visible light, not only for communication but also for localization, has been subject of great interest in research. For systems that require positioning of some sort, the leading technology is the Global Positioning System (GPS) which provides a wide area of coverage at a low cost of implementation. While GPS typically performs well in outdoor environments, it does not provide the level of resolution or reliability needed for indoor localization scenarios [15]. In contrast, the use of visible light allows to obtain precise measurements of received power and angle information from different light transmitters to estimate the position of a receiver with sub-meter accuracy. This is possible by using common localization techniques based on received signal strength (RSS) and angle of arrival (AOA) that we explain in Section 2.3. When compared to the localization accuracy of other technologies such as WiFi (1 - 7 m accuracy) and Bluetooth (2 - 5 m accuracy) for indoors [11], and GPS (5 m accuracy) for outdoors [15], attaining localization errors below 1 m with VLC is a substantial improvement.

In visible light positioning, LEDs (shown in Fig. 2.2a and Fig. 2.2b) are commonly used as transmitters. For sensing, two types of components are often considered: photodiodes (PDs) and CMOS image sensors as shown in Fig. 2.2c and Fig. 2.2d respectively. PDs are mostly used in VLP systems due to their low cost and ease of use. Compared to image sensors they can process data at a higher rate and are more energy efficient, but require the use of multiplexing techniques to identify signals from distinct light sources (we briefly discuss multiplexing in Section 2.4). In contrast, image sensors are capable of capturing multiple pixels of an image in their field of view and can therefore distinguish multiple light sources directly. Despite not requiring the use of multiplexing to identify different transmitters, image sensors are not used as frequently as PDs due to their higher complexity, limited data rate of transmission and higher power consumption [4]. Thus, we will use PDs are receivers for this work.

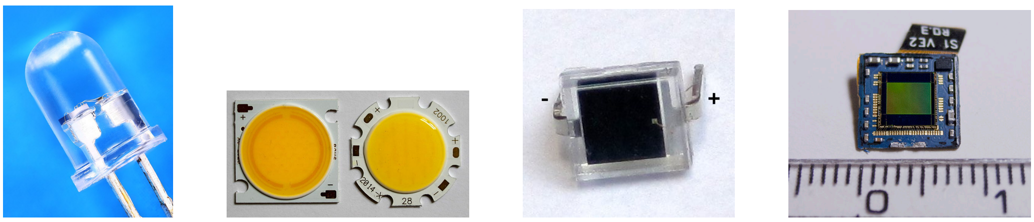

(a) LED (b) High power LEDs (c) PD (d) Image sensor

Figure 2.2: Common hardware elements in VLP systems.

2.2.1 Radiation pattern of light

In VLP, a PD used as receiver (Rx) uses the measured power and angle information of one or multiple transmitters (Tx) as the basis for localization. It is possible to obtain such measurements of RSS (from the received power) and AOA since LEDs are often considered to follow a

Lambertian pattern $R_t(\psi)$ [11], which is determined by the equation below:

$$R_t(\psi) = \frac{m+1}{2\pi} \cos^m(\psi), \tag{2.1}$$

where ψ represents the direction relative to the surface normal of the transmitter, and m represents the Lambertian order. The Lambertian order m determines the width of the beam from the transmitter. A small value of m leads to a wider beam, while a larger m leads to a narrow beam, similar to a spotlight. Formally, the value of m is defined by the semi-angle $\phi_{1/2}$ at half power of the LED and is given by:

$$m = \frac{-ln(2)}{ln(cos(\phi_{1/2}))} \tag{2.2}$$

$\phi_{1/2}$ can be understood as the angle at which the intensity is half of the one found at the axis normal to the surface of the LED. In Fig. 2.3 we illustrate this description.

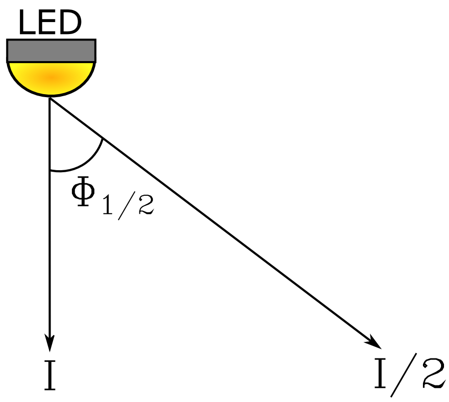

Figure 2.3: Illustration of LED semi-angle $\phi_{1/2}$.

2.2.2 Channel loss model for VLP

The Lambertian pattern $R_t(\psi)$ defines the optical wireless channel between the transmitter and the receiver, which is illustrated in Fig. 2.4 and described by the following equation [16]:

$$H_0(\Theta_c) = \begin{cases} R_t(\psi) \cdot A_\mathrm{r} \cdot \frac{\cos\theta}{d^2} & \text{for } \theta \in [0, \Theta_c], \\ 0 & \text{for } \theta > \Theta_c, \end{cases} \tag{2.3}$$

where d is the distance between the transmitter and the receiver; θ denotes the incidence angle at the receiver; A_r is the effective sensing area of the receiver; and Θ_c represents the field-of-view (FoV) of the receiver, beyond which the receiver is unable to detect the incoming signal.

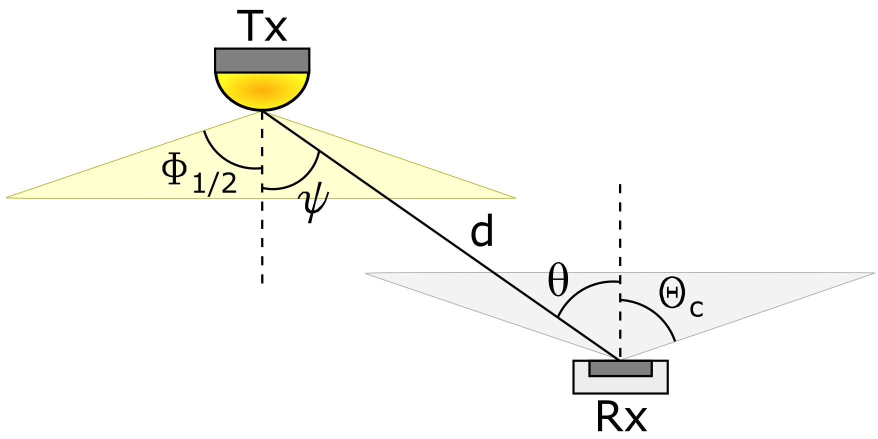

Figure 2.4: VLC system with single transmitter and receiver.

Considering the optical wireless channel, the received power P_r at the PD can be written as:

$$P_r = P_t \cdot H_0(\Theta_c) + N, \tag{2.4}$$

where P_t is the transmitted power and N represents the sum of the shot and thermal noise of the receiver, as well as the ambient noise.

In an ideal environment (i.e. no noise), we may expand Eq. (2.4) to obtain the following equation for the received power:

$$P_r = P_t \cdot A_r \cdot \frac{m+1}{2\pi d^2} \cdot \cos^m(\psi) \cdot \cos(\theta) \tag{2.5}$$

2.3 Localization Algorithms

VLC-based positioning systems can be classified in various ways according to their hardware configurations, multiplexing schemes and other categories. One of the most relevant, is a taxonomy based on the algorithm used for localization [17], as this will heavily influence the hardware requirements of the system and the complexity of the solution. We now present common localization methods and describe their working principles. In Chapter 3, we will use this classification to analyze the state of the art methods and identify which approach is most appropriate considering the unique challenges faced by UAVs.

2.3.1 Received Signal Strength (RSS)

The RSS approach typically uses a Lambertian channel loss model, similar to the one of Eq. (2.3), to obtain the distance between Tx and Rx based on the power of the received signal. When multiple light sources are available, the distance to different anchor points can be estimated and the unique position of the receiver can be obtained via trilateration equations. The trilateration system of equations (also used for GPS) specifies the point of intersection between multiple circles (2D) or spheres (3D) as depicted in figure 2.5. To solve a system of equations using trilateration, a least squares methods is typically employed to obtain the position that minimizes the distance error of the estimation considering the various anchor points. This can be done analytically in one step when sufficient anchor points are available or by using an iterative optimization method. RSS methods are easy and cost efficient to implement but its accuracy tends to be affected by noisy measurements resulting in a lower position accuracy than other techniques.

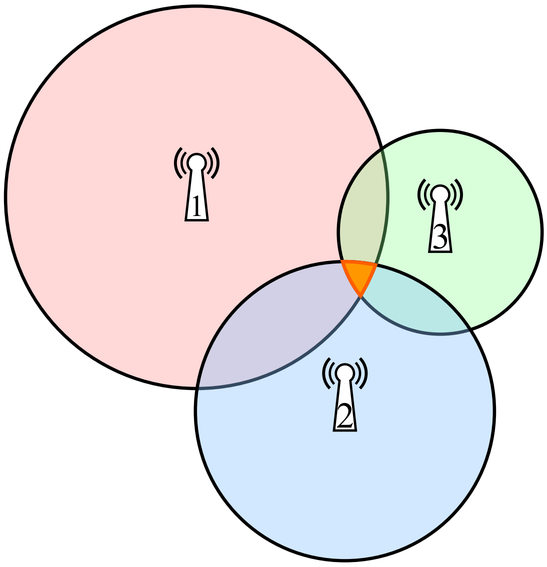

Figure 2.5: Visual explanation of 2D trilateration with multiple antennas.

2.3.2 Time of Arrival (TOA)

The time of arrival method is similar to the RSS approach and it is the basic principle used by GPS. Instead of using the power of the received signal, the timestamp of the signal at departure and arrival is used to determine the distance between two points. In VLP, the distance can be calculated by multiplying the time delay with the speed of light. Evidently, this process can result quite complex in short distances, since it requires accurate synchronization between nodes and a rapid response time of the devices involved.

Although TOA methods are widely used for RF-based positioning, they are not efficient for VLP, particularly indoors, since the speed of light makes the time of arrival measures too short to provide accurate localization [18].

2.3.3 Angle of Arrival (AOA)

As the names suggest, in AOA algorithms, the position of a receiver can be determined utilizing the angle of the signals that arrive from multiple sources. Assuming that the fixed position and angle of more than one ray is known, the location of the receiver can be found at the intersection between two lines as shown in figure 2.6 for the 2D case. AOA methods typically achieve high positioning accuracy, but they present many difficulties in implementation. Multiple receivers, complicated hardware and elaborated mathematical frameworks are often required to obtain angular information, in particular for 3D positioning.

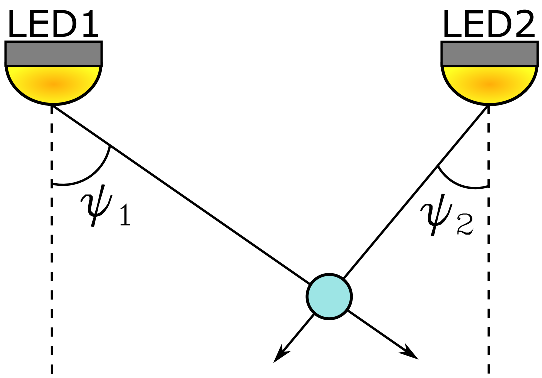

Figure 2.6: Visual example of the principle of a 2D angle of arrival method.

2.4 Multiplexing schemes

In VLP, typically more than one transmitter is necessary to obtain the position of the receiver by an RSS or AOA algorithm. When multiple sources are involved, a multiplexing scheme is required to convey information over a shared medium and avoid interference. VLP systems often require transmitting an ID, the coordinates of anchor points, orientation, or the output power of the source. The most common multiplexing protocols use to convey such information include [10]:

- **Time Division Multiplexing (TDM):** In this technique the signals from the stations are synchronized and transmit data at different times to avoid collisions. It is a simple method to implement, but the synchronization of stations introduces practical complications and the execution of the protocol can be time consuming.
- **Frequency Division Multiplexing (FDM):** The stations transmit light signals at different frequencies and do so asynchronously. This technique reduces complexity on the transmitter's side and leaves it up to the receiver to decode the received information.
- **Code Division Multiplexing (CDM):** A multiplexing technique that encodes data from different sources but is able to transmit over a common frequency band. The protocol is more robust than TDM and FDM but increases the complexity of the implementation.
- **Space Division Multiplexing:** Mainly used for systems with an image sensor where the receiver can discriminate between sources depending on their position in a pixel space.

2.5 VLP for UAVs

In Chapter 1, we mentioned the interest of researchers towards VLP and its use for industrial applications with UAVs. However, available methods for 3D VLP have mostly been tested considering static setups, which neglect the effect of mobile receivers in the performance of the system [4]. This should not be the case in VLP for drones, where the receiver is mobile and has 6 degrees of freedom (DoF), as shown in Fig. 2.7a and Fig. 2.7b. When compared to a static setup, the effect of a mobile receiver introduces two important dynamics in the system: translation and rotation. First, with transitional movements, the distance d to a transmitter changes, affecting the irradiance angle ψ of the optical channel from Eq. (2.3). Second, any transitional movement requires the drone to tilt around its axes, affecting the incidence angle θ. For example, in order to move forward and backward, the drone has to tilt in the pitch axis; and the tilting angle influences the speed of the movement. In combination, these dynamics have a direct effect on the power received, as observed from Eq. (2.5).

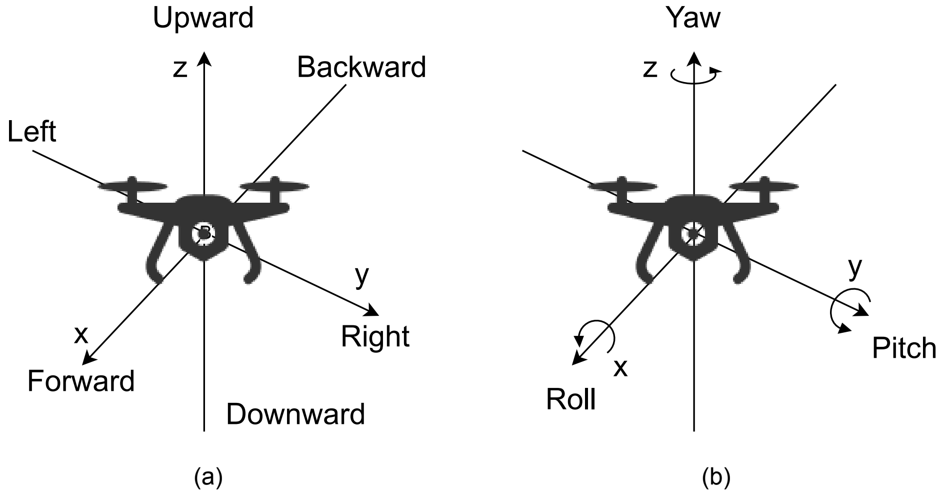

Figure 2.7: Possible (a) transitional and (b) rotational movements of a drone.

Although *some* conclusions can be drawn about the effectiveness of certain approaches, the real challenges of achieving VLP for UAVs remain to be confirmed, since no method has been tested on an actual drone exposed to 6DoF. Based on literature studies, in Table 2.1 we present the main obstacles that could be expected when attempting VLC-based positioning for UAVs. In this work, we only tackle the challenges of mobility, tilting, and hardware constraints as they are the first necessary points to address in order to provide drones localization. In Chapter 3, we take into account these challenges to analyze the available state-of-the-art methods and select the most suitable ones considering a real drone implementation.

Challenge	Description	Study/Source
Mobility	VLC is a highly directional technology which could present problems in applications with high mobility (such as drones) due to speed variations, vibrations, signal fluctuations and interference from obstacles.	[4], [5], [19], [20]
Tilting and 3D dynamics	All drone applications require 3D positioning which involves a complex mathematical framework when compared to the 2D positioning case where the receivers operate at a fixed height. Additionally, many VLP methods assume that the light source and receiver are parallel to each other which is not a valid supposition for accurate UAV positioning.	[13]
Energy constraints	The energy budget in drones is highly restricted and despite the use of low-power LEDs and PDs, it is an important element to take into account. When adding PD interfaces to an already constrained system this could have a detrimental effect in flight time due to the energy consumption and weight capacity of the drone.	[4], [19]
Processing/real-time constraints	The real-time execution of positioning algorithms can be a high-overhead task for embedded processors, such as the one available in a UAV.	[4]
Multipath effects	The reflection of light sources on walls or obstacles can considerably degrade the performance of VLP systems.	[13], [21]
Ill-conditioned scenarios	In environments where line-of-sight or access to visible light access points (VAPs) is temporarily not available, then a unique solution to the positioning problem may not be possible to obtain. In addition, the limited field of view (FOV) of the receiver implies the existence of *dead-zones*, where the minimum amount of signals required to determine location cannot be attained.	[4], [6], [22]

Table 2.1: Summary of challenges of VLP for UAV applications.

3 ANALYSIS

In this chapter, we introduce the available VLP techniques in three categories: AOA-based 3D, RSS-based 3D and RSS-based 2D+H. We analyze the feasibility of each category for drone localization using the following criteria:

- The complexity of the receiver design considering the limited weight capacity and power budget of drones.
- The complexity of the algorithm, that affects the processing, memory and power requirements in the constrained environment of the drone.
- The complexity of the transmitter design, critical to transform our lighting system with minimal changes.
- Whether tilting is considered, which is important for mobile scenarios as discussed in Chapter 2.

3.1 3D VLP with AOA

In previous studies, AOA-based methods have shown to be more accurate than RSS-based methods for 3D VLP in simulation and experimental evaluations in static conditions, achieving sub-decimeter levels of accuracy in certain scenarios [23, 24, 25]. However, AOA-based methods have considerably higher complexities in terms of the required infrastructure support, the underlying mathematical framework and the computational complexity.

In the design by Yang et al. [25], and the design by Xie et al. [26], multiple PDs are arranged at different angles in polygonal structures to allow the use of both AOA and RSS information to uniquely determine the position of a receiver. The requirement of using multiple PDs placed at different angles increases the profile of the receiver significantly and may not be feasible on small drones. In Fig. 3.1 we show an example of a PD structure, which is similar to the ones often required by AOA methods considering more than one PD.

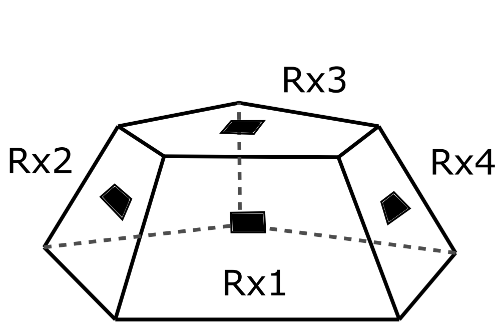

Figure 3.1: Multiple PD structure for AOA systems.

In the design by Sahin et al. [23], the complexity of design is transferred from the receiver to the transmitter by proposing the use of Visible Light Access Points (VAPs). VAPs consist of multiple tilted LEDs, which are used to provide AOA information to a single receiver sensor on the drone. An example of such VAP is shown in Fig. 3.2a where multiple transmitters are visible from the bottom view. In Fig. 3.2b we can see from the lateral section view that LEDs in the periphery have an angle *A* with respect to the LED in the center, which results in a complex transmitter design to implement at scale.

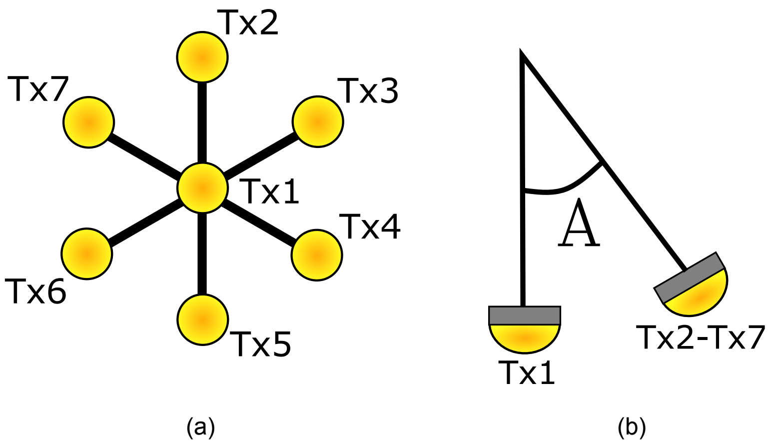

Figure 3.2: Visible light access point (a) bottom view and (b) lateral section view.

In the design by Zhu et al. [24], very accurate results are reported based on the angle difference of arrival (ADOA) information. However, in addition to using a PD array, a complex framework is also required, which results in a high computation time even on a dual-core 2.4 GHz processor.

In summary, AOA-based methods can achieve a high accuracy but require either complex receiver designs and algorithms, which are infeasible for small drones; or elaborated and costly transmitters, which do not scale well to a large lighting infrastructure.

3.2 3D VLP with RSS

Compared to AOA-based methods, RSS-based methods require considerably less infrastructure but impose some stringent constraints on the evaluation setup. For example, in the study by Li et al. [16] and the study by Zhuang et al. [20], the receiver and the transmitter are assumed to be parallel to simplify the problem as depicted in Fig. 3.3. Even though the design implementations have lower complexities, the parallel assumption is unlikely to remain valid when drones are flying. In the study by Cai et al. [27], a 3D RSS-based VLP method is demonstrated with an average error of a few centimeters. However, a computationally intensive particle swarm optimization (PSO) algorithm is adopted to solve for the position. In addition, the experimental scenarios consider that receivers remain static and parallel to the transmitters. In the study of Carreño et al. [28], the computationally-heavy Genetic Algorithm (GA) and PSO are considered to solve the 3D VLP problem and report comparable accuracy results to [27] for both algorithms.

In summary, RSS-based methods have potential for 3D VLP for drones, as they require less hardware elements compared to AOA-based methods. However, the main shortcomings are their computationally intensive optimization algorithms and the fact that the methods are accurate only with *static* receivers maintaining a *parallel orientation* with the transmitters.

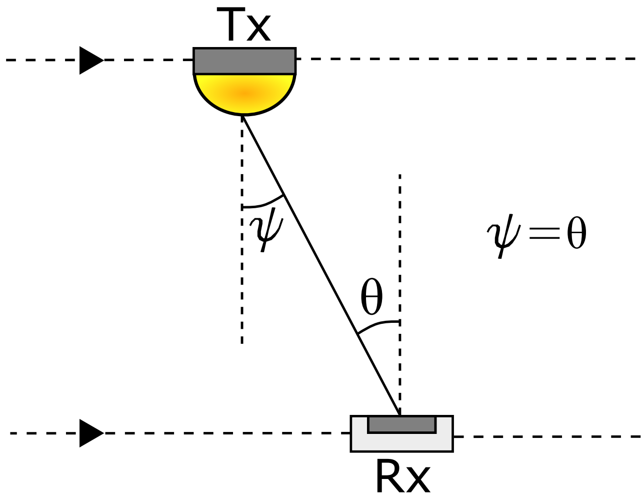

Figure 3.3: Parallel Tx-Rx assumption (black arrows denote parallel lines).

3.3 2D+H VLP with RSS (Indirect-H)

A promising approach in using RSS-based methods for 3D VLP is to decompose the problem space into *2D+H*, where the height (H) and the 2D position of the receiver are independently estimated. For example, in the studies by Plets et al. [12] and by Alamadani et al. [13], a list of different height values are sequentially assumed, and for each height, the 2D position is solved via trilateration. After the trilateration process is completed for all different heights, the algorithm then determines which height is the most probable to be correct by minimizing the error of a cost function that identifies which candidate solution is the most likely. Both studies are able to achieve 3D VLP with modest infrastructure and algorithmic complexities, and report favorable results for *static* receivers that are parallel to the transmitters. In the study of [13], however, when tilting is introduced, the positioning error of their method increases more than 15 times when the inclination is 3° and more than 30 times when it is 5°. In addition, the experiments are performed in a controlled environment using a high-end PD, which does not reflect the normal working conditions of drones.

A key problem of 2D+H methods is that they use an *indirect* approach to estimate height. Height is obtained through RSS measurements. This approach works well with parallel and static receivers, but mobility and tilting affect their performance. We use these studies as the baseline of comparison for our proposed method in Chapter 4, and for the remainder of the thesis we will refer to 2D+H Indirect methods as Indirect-H.

3.4 Comparison of SoA methods

To conclude this chapter, we show the performance of the discussed SoA methods in terms of accuracy (reported positioning error) and the LED density in Fig. 3.4. The density of anchor

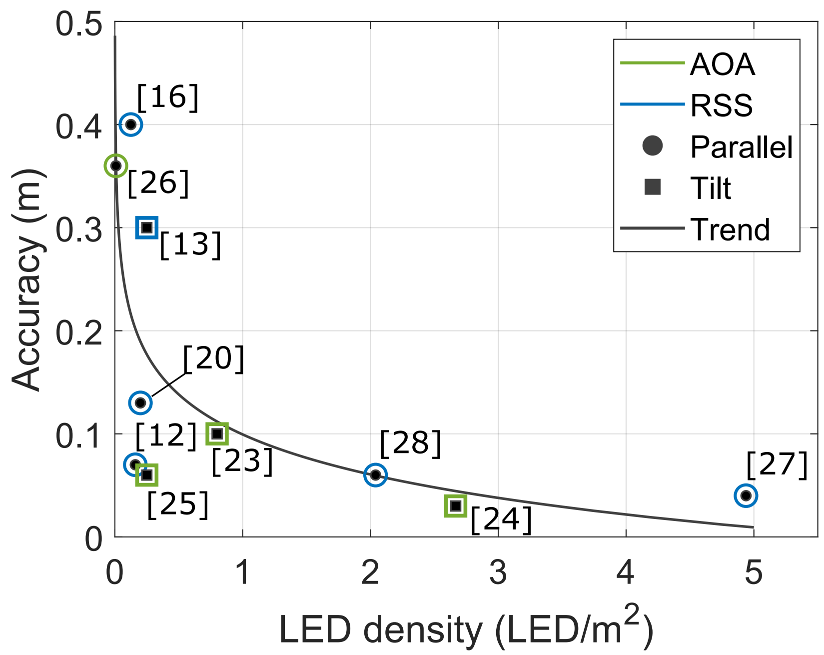

Figure 3.4: Accuracy vs LED density for different SoA studies. The curve represents the average trend of SoA studies.

points is a major indicator of how well a VLP system will perform and provides a basis for comparison [4]. The methods are categorized by type (AOA or RSS) and testing conditions (if the receivers are *parallel* to the transmitters in their evaluations or if they consider *tilted* setups). All these studies, including the ones evaluating tilting, consider only *static* receivers in their experimental evaluations.

We can see from Fig. 3.4 that in general, a lower LED density has a detrimental effect in the accuracy that can be achieved and vice versa. When considering all studies, AOA methods appear at or below the trend line and achieve the lowest positioning error despite being evaluated with tilted receivers. Some RSS methods also perform comparably well, but only consider the parallel case between transmitters and receiver. Finally, the study of [13] performs worse than other RSS methods with comparable LED density since it is the only one that considers tilt in their experimental evaluations.

In order to have a high localization accuracy for drones while keeping the hardware complexity low, we consider RSS methods in favor of the AOA approach. In Chapter 4, we build upon the 2D+H framework and propose Firefly, where we use available sensors in the UAV to overcome the limitations of the SoA that only considers parallel transmitters and receiver. In Chapter 6, we compare Firefly against two other SoA approaches in a significantly more challenging *mobile* scenario.

4 SYSTEM MODEL

In Firefly, our aim is to keep the hardware complexity as low as possible. Therefore, we consider an infrastructure where each LED transmitter has a single off-the-shelf light with no tilted or custom-made structure. This maintains the simplicity of the transmitters, making them easily scalable. Similarly, on the receiver side, our design requires each drone to be equipped with only a single PD for VLP. Based on the analysis of Chapter 3, we consider the Indirect-H methods from [12] and [13] as the initial building block of our model. Even though these methods require that the transmitter and receiver are parallel to each other to obtain an accurate positioning result, they have low hardware and algorithmic complexities.

In this chapter, we first explain how we obtain the RSS and identifier (ID) of light source, which are pre-requisites for RSS methods. Then we explain the common framework, assumptions and limitations of RSS methods; and in particular the Indirect-H approach. Finally, we explain the localization method proposed in Firefly and the necessary modifications to the common framework that enable accurate VLP in a mobile scenario with 6 DoF.

4.1 Obtaining RSS and ID of LED transmitters

In VLP systems, the information that is conveyed to the receiver in order to obtain its location varies. Common examples include broadcasting the output power, lambertian order, position and orientation of the transmitter. In Firefly, we keep a minimal approach where we assume that the parameters of the PD receiver and LED transmitters are known (i.e. m, A_r) from the data sheet of the manufacturer and do not need to be transmitted. This allows for a simple implementation where only the RSS is required from the transmitter and the other parameters (ψ and θ) are obtained using available sensors on the UAV.

4.1.1 ID selection

For the localization method to work, however, it is also necessary to know which RSS corresponds to which transmitter. For this purpose, we use frequency division multiple access (FDMA) to transmit the ID of different LEDs simultaneously. In FDMA, a unique ID is generated by turning on and off the LEDs at a selected frequency. This results in a square wave signal generated by each transmitter. The combined signal can then be sampled by a single PD in the receiver, and decomposed by a Fast Fourier Transform (FFT) to obtain the RSS (P_r) corresponding to a unique light source.

The choice of FDMA simplifies the complexity of the implementation, as LEDs can transmit without the need of synchronization, and using a shared medium. In addition, with the FDMA approach, the FFT will isolate sources of high frequency noise (such as shot and thermal noise) as well as the constant DC component of ambient light to obtain a clean RSS signal. In turn, this makes our system resilient and capable to operate in dark and illuminated environments

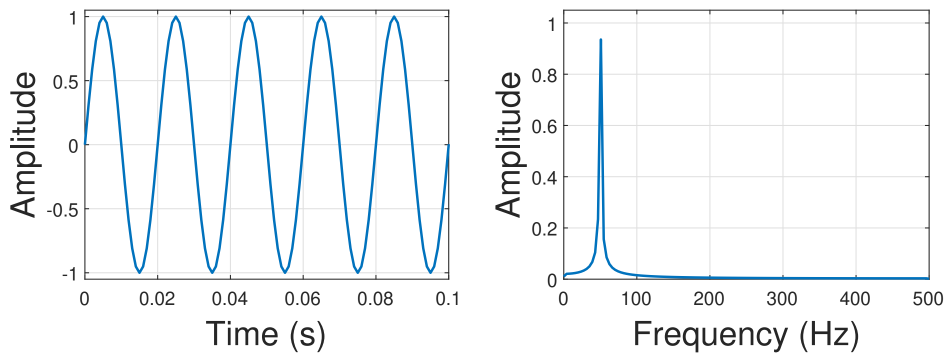

(a)

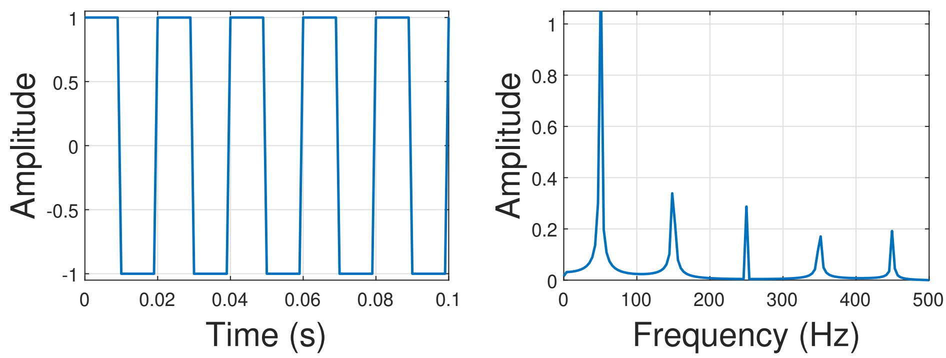

(b)

Figure 4.1: Time and frequency domain graphs (after FFT) of a 50 Hz (a) Sine wave and (b) Square wave.

with a simple implementation (i.e. no additional synchronization protocol is required).

When using the FFT to obtain the RSS information from a square wave, some considerations have to be taken into account. To clarify our approach, Fig. 4.1a shows the time and frequency domain graph of a 50 Hz sine wave with an amplitude of 1. In the case of a sine wave, a single peak can be appreciated in the frequency domain. In contrast, a square wave of the same frequency and amplitude characteristics, will present multiple peaks in the frequency domain as shown in Fig. 4.1b. This can be explained by the Fourier series of a square wave:

$$x(t) = \frac{4}{\pi} \sum_{k=1}^{\infty} \frac{sin(2\pi(2k-1)ft)}{(2k-1)} \tag{4.1}$$

From Eq. (4.1), we see that the square wave contains only odd-integer harmonics corresponding to the $2k-1$ term. Harmonic components can be a source of possible interference between transmitters and should be avoided. A simple solution, first proposed by [29], is to select IDs that are 2^n multiples of a selected base frequency f_0 (i.e. $2f_0, 4f_0, 8f_0, etc.$). Any base frequency of the system can be chosen as long as the hardware limitations of the receiver and transmitters are taken into account. In VLC systems, frequencies above 200 Hz are preferred as they are generally regarded as safe for humans and will not result in any disturbance [11] .

4.1.2 RSS

By looking at Fig. 4.1a and Fig. 4.1b, we can also observe that the amplitude of the sine and square waves is noticeably different. From Eq. (4.1) and for $k = 1$ (the term that corresponds to the frequency IDs), the amplitude of the square wave signal is multiplied by a factor of $\frac{4}{\pi}$. To retrieve the magnitude of the original time domain signal it is sufficient to multiply the measured RSS by the reciprocal (i.e. $\frac{\pi}{4}$).

As a final consideration, we see from Fig. 4.1a that even for the sinusoidal signal, the magnitude in the frequency domains is slightly lower than 1. This is the result of performing a discrete Fourier transform where some of the received power of the signal *leaks* into adjacent frequency bins. This phenomenon is known as *spectral leakage* and can be mitigated by increasing the number of samples in the FFT, performing *Zero-Padding* or adjusting with a calibration factor.

In summary, the ID and RSS values of multiple transmitters is obtained using FDMA and taking into account simple considerations. Namely, the frequency IDs must be a 2^n multiple of a selected base frequency and the retrieved RSS value must be multiplied by a factor of $\frac{\pi}{4}$.

4.2 Common framework of RSS methods

As described in Section 4.1, we assume that the parameters from the data sheets of the LED transmitters and PD receiver are known. Therefore, with the RSS information, the distances between the transmitters and the PD on a drone can be calculated directly from Eq. (2.5), if the incidence angle θ and irradiance angle ψ are also known. A common assumption in the SoA studies, including Indirect-H methods, is:

- Assumption 1 (A1): The transmitters and receivers are parallel (||).

This assumption greatly simplifies the problem and leads to the following equation:

$$cos(\psi) = cos(\theta) = \frac{|z_r - z_i|}{d_{i,\|}} = \frac{h}{d_{i,\|}}, \tag{4.2}$$

where z_r denotes the height of the receiver; z_i represents the height of the *i*-th transmitter; h is the height difference; and $d_{i,\|}$ is the distance between the receiver and the *i*-th transmitter. In Fig. 4.2, we show the reference and parameters of the system for clarity.

By substituting Eq. (4.2) into Eq. (2.5), the distance between the receiver and the *i*-th transmitter is given by:

$$d_{i,\|} = \left[\frac{P_{t,i}A_r(m+1)h^{m+1}}{2\pi P_{r,i}}\right]^{\frac{1}{(m+3)}} \tag{4.3}$$

With this method, a good accuracy can be obtained when A1 is true [12]. However, the study of [13] shows that when RSS is used to estimate height, the result is affected by tilt of the receiver. In turn, this has a considerable effect in the overall accuracy of the method. Thus, the Indirect-H approach is inadequate when assumption A1 is broken. We address the limitations of the Indirect-H method to achieve accurate localization, even when A1 does not hold true.

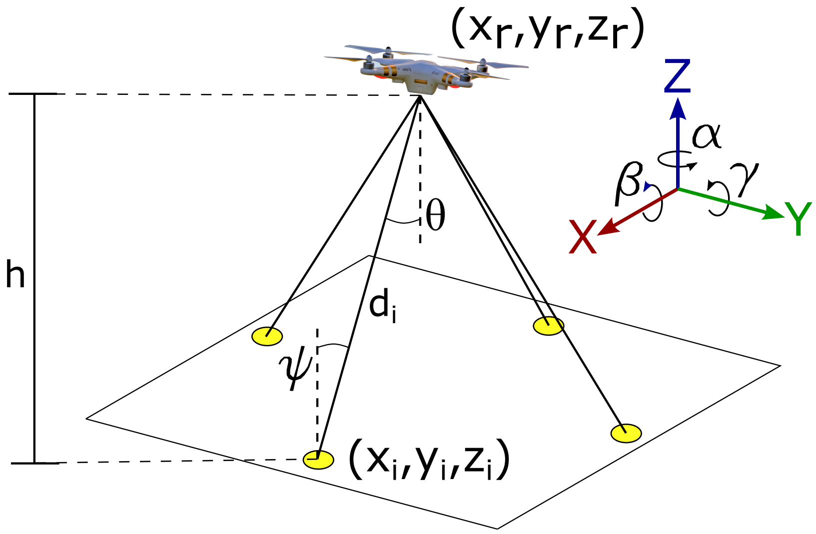

Figure 4.2: System reference and parameters. Without loss of generality, we place the LEDs (transmitters) on the ground.

4.3 Firefly

In Firefly, we adopt a multi-sensor fusion approach. We design a *direct* height estimation method that is robust against tilting using both inertial sensors (IMUs) and barometric sensors. As most off-the-shelf drones are already equipped with both kinds of sensors, no additional hardware is needed. We directly introduce our estimated height into the distance equations of the common framework and perform two iterations of 2D trilateration, as shown in Fig. 4.3, to obtain a better approximation of the irradiance and then the incidence angles. Our method consists of three steps summarized hereafter:

- *Step 1:* The height of the drone is measured using the onboard barometer and IMU with a complementary filter. The Indirect-H method proposed in SoA studies is applied to correct the long-term zero drift of the barometer.
- *Step 2:* We perform a *first iteration* of the 2D trilateration method assuming that the transmitters and receiver are parallel. These (initial) location estimate provides a good approximation of the irradiance angle and serves as a basis for Step 3.
- *Step 3:* Taking into account the tilting of the drone obtained from the IMU (incidence angle), we perform a *second iteration* of the 2D trilateration method, which gives us the final localization result.

4.3.1 Step 1: Height estimation

To obtain a reliable measurement of the height of a drone, two types of sensors are often considered: IMUs and barometric sensors. IMUs consist of accelerometers and gyroscopes that are used to track the position and orientation of an object. Their low costs, form factors and power consumption make them an ideal option for drone navigation. While IMUs are good at measuring instantaneous changes, their outputs are prone to noise and drift errors, even over a short period of time. By using only inertial sensors for positioning, it has been shown that the positioning error can reach over 10 m after 2 s and over 150 m after 60 s [30]. On the other

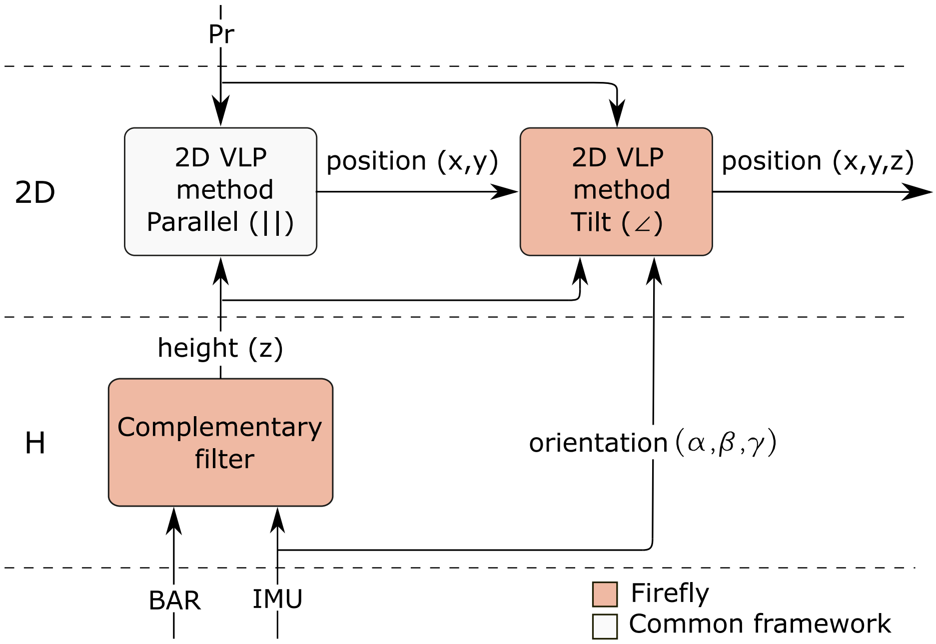

Figure 4.3: Firefly approach. The common framework of the SOA, which assumes a parallel setup, is enhanced with two novel components: a direct measurement of height via a complementary filter and a 2D VLP method that considers tilt.

hand, the output of barometers, which use air pressure to measure altitude, is sensitive to rapid variations in the air pressure uncorrelated with altitude changes. However, over a longer time period, barometers can provide a stable estimate of height.

Considering that the strengths of both kinds of sensors are complementary, their respective advantages can be *fused* to obtain an improved measurement using the *long term* reference of the barometer and the *short term* agility of the acceleration measurements. In Firefly, we adopt the complementary filter from [31], to apply a high-pass filter to the vertical acceleration from the IMU and a low-pass filter to the output of the barometer. The complementary filter is especially suitable for a resource-limited UAV, compared to other sensor fusion methods such as the Kalman Filter, because of its simplicity. The following discrete equations are used for the complementary filter to obtain the height z_r and speed of the receiver $\dot{z}_r$:

$$\hat{z_n} = \begin{bmatrix} z_r \\ \dot{z_r} \end{bmatrix} = \begin{bmatrix} 1 & T_s \\ 0 & 1 \end{bmatrix} \hat{z}_{n-1} + \begin{bmatrix} 1 & \frac{T_s}{2} \\ 0 & 1 \end{bmatrix} k_f T_s \Delta z_{n-1} + \begin{bmatrix} \frac{T_s}{2} \\ 1 \end{bmatrix} \Delta v_{n-1} \tag{4.4}$$

where

$$\Delta z = h_{bar} - z_r$$

$$\Delta v = a_z T_s$$

considering that the n sub-index denotes the current iteration; h_{bar} is the height measurement of the barometer; a_z is the vertical acceleration obtained from the IMU; and k_f is the complementary filter gain, which can vary depending on the noise of the sensors used. From the discrete equations we see that the height z_r is influenced by the previous state (position and velocity), and updated with information from the barometer and accelerometer at each time step Ts.

When combined with inertial sensors, barometers can provide accurate height estimation for drones, for example, with errors of less than 15 cm after 3 min [32]. Nonetheless, due to changing conditions in the environment, barometers are likely to eventually drift from the initial conditions set during calibration. This is also known as *zero drift*. One possible solution to correct the zero drift is to perform frequent calibrations at defined locations or checkpoints, but this approach is cumbersome. In Firefly, we propose a simple zero drift correction scheme using VLP, which is shown in Fig. 4.4.

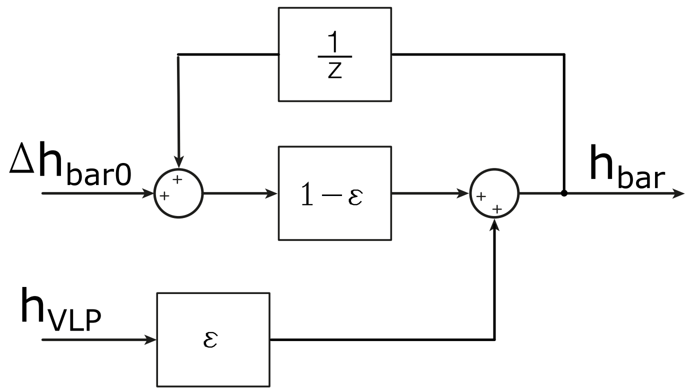

Figure 4.4: Block diagram for barometer drift correction scheme.

As described in Sec. 3, the Indirect-H method already provides a solution to indirectly estimate the height of a drone using VLP. This solutions is not accurate when tilting occurs, but provides a drift-free height measurement. Thus, we use the Indirect-H measurement to correct the drift problem, but only when it can be trusted, i.e. when the roll and pitch angles of the drone are below a threshold such as 3° using information from the IMU.

In our method, the height estimated by the Indirect-H VLP is denoted as h_{VLP}, and the change of height measured by the barometer is denoted as Δh_{bar0}. Overall, Δh_{bar0} has a higher accuracy than h_{VLP} to detect changes in altitude and we show this in Chapter 6. The measurement results h_{VLP} and Δh_{bar0} are then scaled by a constant ϵ and $1-\epsilon$, respectively, to obtain the final height estimation h_{bar}. In the following iterations, h_{bar} then acts as a correction for Δh_{bar0}. By choosing a small value for the constant ϵ, the Indirect-H height estimation (h_{VLP}) has a minor influence in the immediate output. This ensures that the height estimation is still accurate. At the same time, the drift-free h_{VLP} has an anchor effect on the long term, which corrects zero drift from the barometer. Together with the IMU data, h_{bar} is the input to the complementary filter.

4.3.2 Step 2: Parallel Tx-Rx

In the previous step, we directly obtain the height z_r of the receiver. Now, we utilize this accurate height to obtain a first estimation of the x_r and y_r coordinates of the receiver. This step tackles the issue caused by the incorrect characterization of the irradiance angle in Indirect-H. By directly estimating height, we obtain a better approximation of the irradiance angle than the Indirect-H method. For this first iteration, we consider the common framework of RSS methods where the receiver is parallel to the transmitter. We take into account the effect of the tilt of the drone (incidence angle) in the next step.

In a typical indoor environment the transmitters are fixed, and the irradiance angle ψ is not affected by tilting of the receiver. Then, for the irradiance angle, Eq. (4.2) is valid and we can use Eq. (4.3) to obtain distance, provided that the height estimation is accurate. Note in Fig. 4.5 that given an estimation of d_i (based on RSS measurements), a correct height is critical to obtain a proper characterization of ψ, and that is the main strength of Firefly compared to Indirect-H. With the distance and the height estimation we can obtain the position of the drone using a standard trilateration procedure. In our system, as we are using visible light for positioning, we can consider the main sources of noise to be the shot and thermal noises [33]. Therefore, we adopt the maximum likelihood estimation (MLE) to perform 2D trilateration, as it takes into account statistical considerations to minimize the error of noisy measurements [34].

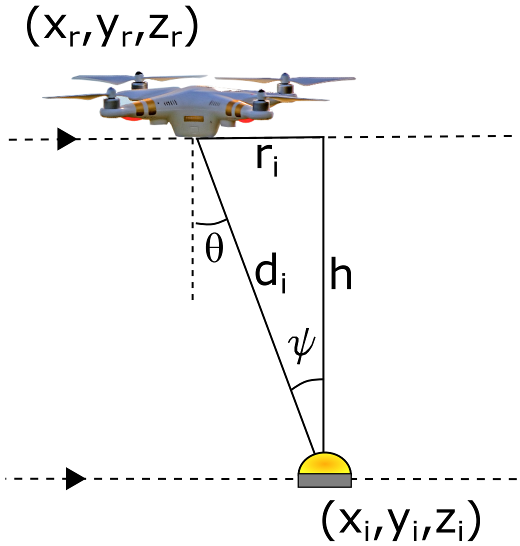

Figure 4.5: Lateral view of system reference and parameters.

The MLE method finds the most likely position of the receiver at the intersection of i circles with radius r_i, corresponding to the horizontal distance of the drone to our i anchor points (at least 3). Since we have already obtained the distance d_i to each anchor point and the height z_r of the receiver, it can be observed from Fig. 4.5 that by using the Pythagorean theorem, the radius of each circle in the 2D plane is simply:

$$r_i = \sqrt{(d_{i,\|}^2 - h^2)} \tag{4.5}$$

We can now obtain the 2D position of the receiver (x_r, y_r) by solving the following system of equations from the MLE method:

$$X = \begin{bmatrix} x_r \\ y_r \end{bmatrix} = (A^T A)^{-1} A^T B \tag{4.6}$$

where

$$A = \begin{bmatrix} 2(x_1 - x_i) & 2(y_1 - y_i) \\ \vdots & \vdots \\ 2(x_{i-1} - x_i) & 2(y_{i-1} - y_i) \end{bmatrix} \tag{4.7}$$

$$B = \begin{bmatrix} x_1^2 + y_1^2 - r_1^2 - (x_i^2 + y_i^2 - r_i^2) \\ \vdots \\ x_{i-1}^2 + y_{i-1}^2 - r_{i-1}^2 - (x_i^2 + y_i^2 - r_i^2) \end{bmatrix} \tag{4.8}$$

considering that x_i and y_i are the coordinates of the i-th transmitter.

4.3.3 Step 3: Tilting of the receiver

In the previous step, we obtain the position of the receiver assuming that the incidence and irradiance angles are equal. As we explained before, the irradiance angle is not affected by tilting in our setup. In contrast, the incidence angle θ is directly influenced by the 3D orientation of the receiver. We can obtain orientation information using the IMU which we already use to estimate the height of the drone. In this step, we perform an additional iteration of the 2D MLE method, using distance measurements that account for tilt ($\angle$). From equation Eq. (2.5) we have:

$$d_{i,\angle} = \sqrt{\frac{P_{t,i}A_r(m+1)cos^m(\psi)cos(\theta)}{2\pi P_{r,i}}} \tag{4.9}$$

where the irradiance angle ψ is described by equation Eq. (4.2) and the incidence angle θ is described by [25]:

$$\theta = cos^{-1}\Big(\frac{\theta_x + \theta_y + \theta_z}{d_{i,||}}\Big) \tag{4.10}$$

with

$$\theta_x = (x_r - x_i)cos(\gamma)sin(\beta)$$

$$\theta_y = (y_r - y_i)sin(\gamma)sin(\beta)$$

$$\theta_z = (z_r - z_i)cos(\beta)$$

where γ, β are the roll and pitch Euler angles respectively obtained from the IMU. We can see from Eq. (4.10) that the first iteration of the 2D trilateration method (Step 2) is necessary since the position of the receiver (x_r, y_r and z_r) is required in addition to its orientation for θ_x and θ_y.

With the previously described steps, we can overcome the limitations of the Indirect-H method when tilting occurs. By directly estimating height we achieve a better approximation of the irradiance angle and by utilizing sensors from the IMU, the incidence angle is obtained. In the following chapter we discuss the details of implementation of Firefly in an experimental testbed that considers a real drone with 6 DoF.

5 IMPLEMENTATION

As we have mentioned in Chapter 3, the literature mostly considers static receivers in their experimental validations and no study tests mobile receivers subject to 6DoF. In the case of drones, it is important to test the performance of the proposed method in a real scenario due to the mobility and tilting involved in drone applications. In this chapter, we provide details of implementation for the testbed for our system that considers a 3D mobile environment with tilting of the receiver.

We first provide an overview of the system for clarity. Then we explain the hardware implementation for the main components of the system, and finally, we detail the pieces of software that enable the flow of information between parts.

5.1 Overview of the testbed

We build a testbed in a 2 m $\times$ 2 m $\times$ 2 m indoor environment as shown in Fig. 5.1a. The testbed has three main components: 1) 4 transmitting LED sources located at fixed positions, 2) the drone, and 3) a ground truth system to determine and control the drone's position during flight. The connection between these components and the schematic overview of their functionalities are shown in Fig. 5.1b. The configuration of the system is listed in Table 5.1.

<table>
<tr><th>Parameter</th><th>Label</th><th colspan="2">Value</th></tr>
<tr><td>Testbed size</td><td>-</td><td colspan="2">2 m $\times$ 2 m $\times$ 2 m</td></tr>
<tr><td rowspan="4">Position (x, y, z) and frequency ID of each transmitter</td><td>Tx_1</td><td>(0.25 m, 1 m, 0 m)</td><td>60 Hz</td></tr>
<tr><td>Tx_2</td><td>(1 m, 1.75 m, 0 m)</td><td>120 Hz</td></tr>
<tr><td>Tx_3</td><td>1.75 m, 1 m, 0 m)</td><td>240 Hz</td></tr>
<tr><td>Tx_4</td><td>(1 m, 0.25 m, 0 m)</td><td>480 Hz</td></tr>
<tr><td>LED power</td><td>P_{nom}</td><td colspan="2">2.7 W</td></tr>
<tr><td>Lambertian order</td><td>m</td><td colspan="2">14</td></tr>
<tr><td>Area of the PD</td><td>A_r</td><td colspan="2">5.2 mm^2</td></tr>
<tr><td>FOV of the PD</td><td>Θ_c</td><td colspan="2">80°</td></tr>
</table>

Table 5.1: Parameters of the system.

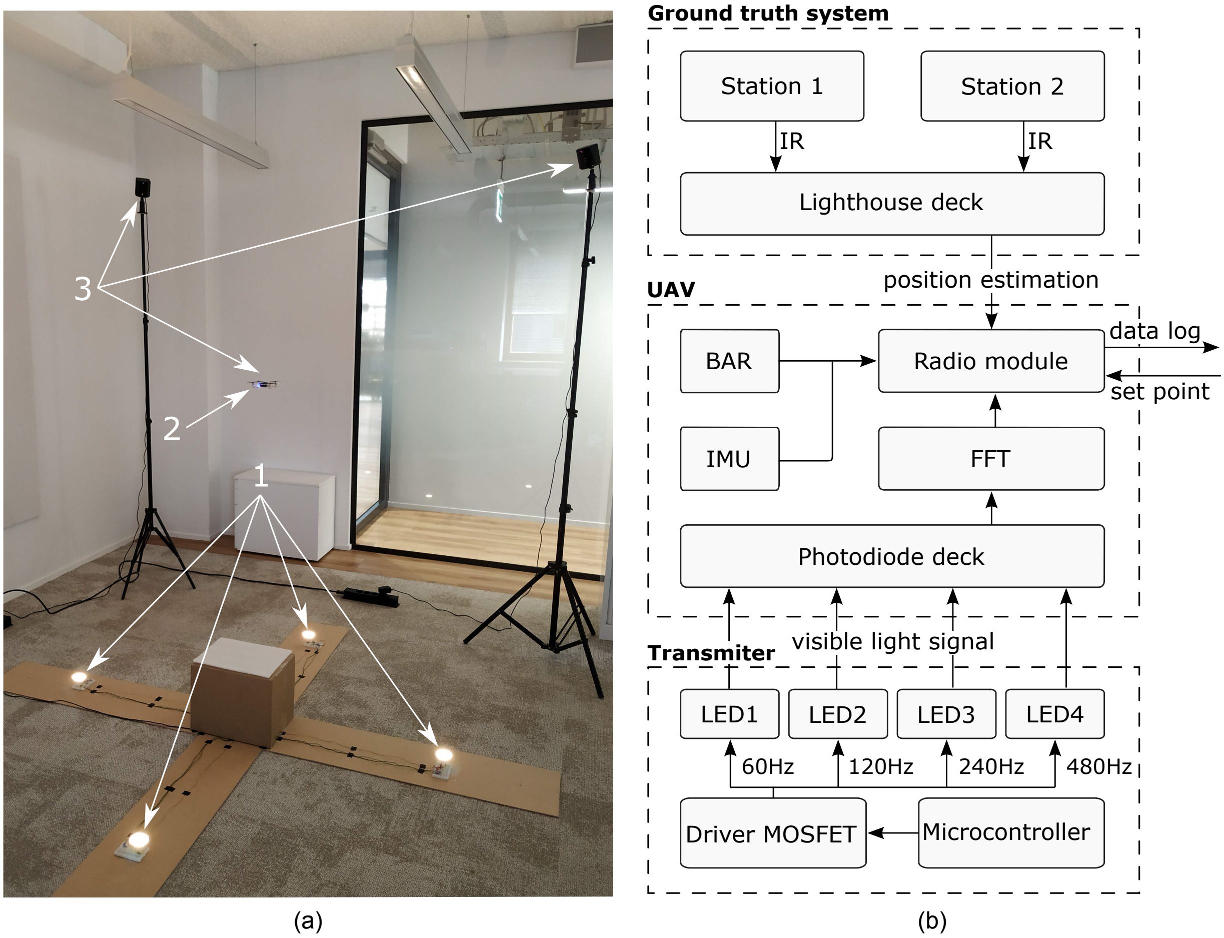

Figure 5.1: The overview of the system. (a) The physical position of the testbed with 1) 4 transmitters; 2) UAV; and 3) the ground truth system. (b) Schematic overview of the connection and functionalities of the components.

5.2 Hardware implementation

5.2.1 Transmitter

We use the CorePro LEDspot LV lamps as transmitters which are connected to a MOSFET transistor and controlled by a microcontroller as shown in Fig. 5.2. In order to generate a unique frequency identifier (ID) we used the FDMA scheme explained in Section 4.1. In our system, the base frequency f_0 of 60 Hz is chosen for evaluation, however, any f_0 can be used considering the hardware limitations of the transmitters and the receiver. Then, the frequency IDs of the LEDs of our system are 60 Hz, 120 Hz, 240 Hz and 480 Hz.

In our setup, we drive the LEDS at 2.7 W. The duty cycle of the square wave used to generate the frequency ID is 50%, and thus the average transmitting power is given by:

$$P_t = P_{nom} \cdot D \tag{5.1}$$

where P_{nom} is the nominal power of the LEDs and D is the duty cycle. Resulting in a transmitting power of 1.35 W for each lamp.

The beam angle of the LEDs is $36°$ and is provided by the manufacturer in the data sheet. This results in a semi-angle $\phi_{1/2}$ of $18°$ and a Lambertian order of $m = 13.81 \approx 14$ according to Eq. (2.2).

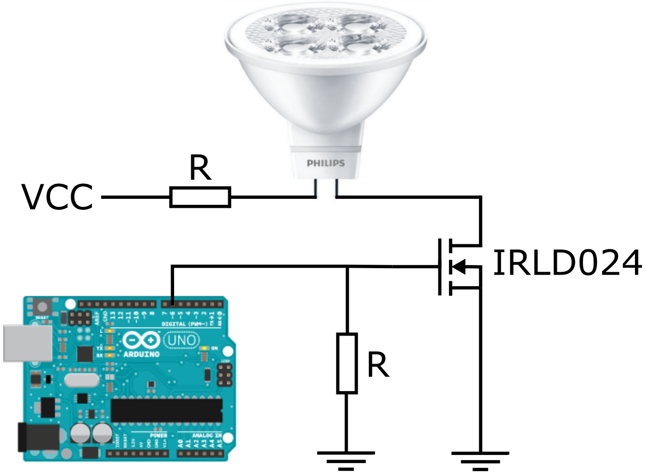

Figure 5.2: Driver circuit for LED transmitters.

5.2.2 Receiver

We select the Bitcraze Crazyflie 2.1 as the receiver. It is a lightweight commercially available drone with multiple peripherals, which makes it easy to attach dedicated or customized hardware to perform different functions. To enable VLP on the drone, an OPT101 photodiode is attached via a custom PCB as shown in Fig. 5.3b. The PD is connected to a 12-bit analog-to-digital converter (ADC) on the Crazyflie.

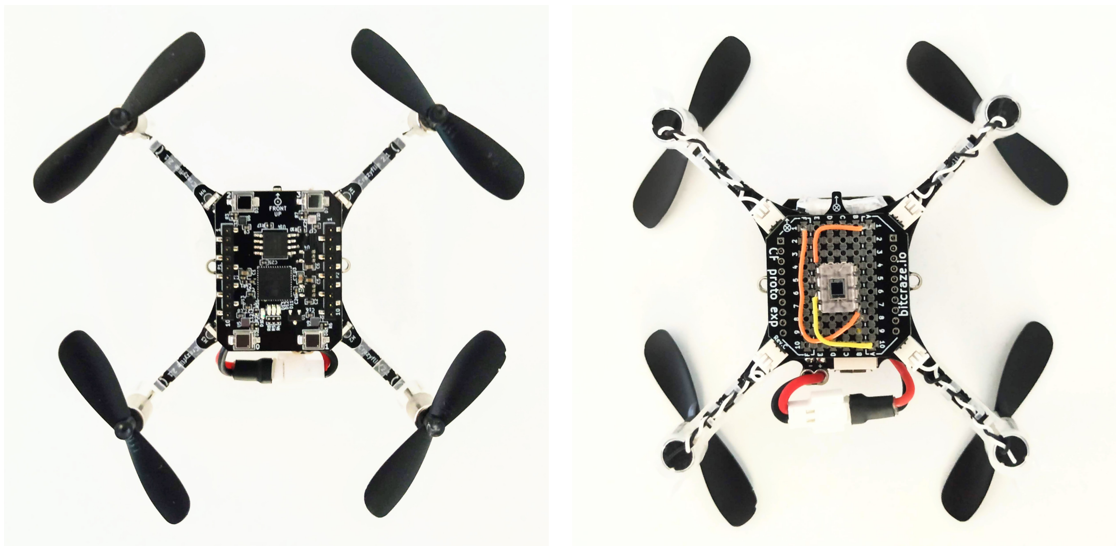

(a) (b)

Figure 5.3: Crazyflie 2.1 mini-drone (a) Lighthouse deck used for ground truth (top view) and (b) custom PD deck (bottom view).

The OPT101 PD shown in figure Fig. 5.4a has been successfully used and tested in multiple VLC projects, such as the OpenVLC 1.3 shield [35], and its sensitivity can be adjusted to match the power requirements of the applications by attaching a variable resistor. In Fig. 5.4b we show the sensitivity configuration chosen for our system using the data sheet information of the manufacturer. Considering the ADC voltage reference of 3 V from the the Crazyflie and using a 100 kΩ resistor, we see that it is possible to measure a radiant power from the transmitter up to around 80μW. This is an appropriate configuration for our system considering the characteristics of our LED transmitters and the dimensions of our setup. For example, we may place the receiver in direct line-of-sight (i.e. when $\psi = 0°$ and $\theta = 0°$) at a distance from the transmitter of 0.5 m or above without saturating the PD. In Chapter 6, we design our flight route taking into account the radiant power that can be sensed and the field of view (FOV) Θ_c of the PD.

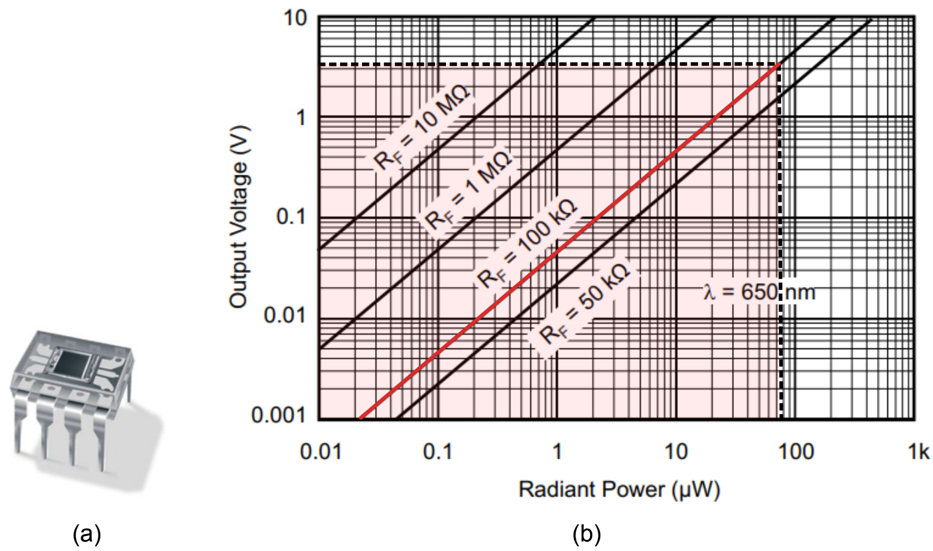

Figure 5.4: (a) OPT101 photodiode and (b) sensitivity configuration.

In figure Fig. 5.5 we show the schematic of the PCB used to connect the OPT101 to the pins pf the Crazyflie. By attaching an external resistor we can modify the default light sensitivity of the PD.

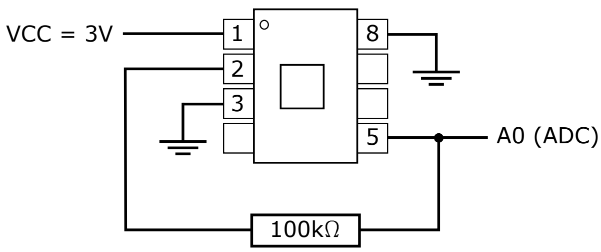

Figure 5.5: PCB schematic of PD deck using an OPT101.

5.2.3 Ground truth system

We use the Lighthouse positioning system from Bitcraze to control and retrieve the ground truth position of the UAV. It consists of two parts: the Steam VR Stations positioned above the flying range of the receiver and the positioning deck attached to the top of the Crazyfile, as shown in Fig. 5.3a. The ground truth system uses the two infrared (IR) stations from Fig. 5.1a to locate the positions of the drone and provides a high accuracy of less than 10 cm. When compared to our proposed VLP system, these dedicated hardware stations present the following disadvantages:

1. Are more expensive (cost more than $200 USD per station compared to less than $5 USD for an LED lamp).
2. Require careful setup and calibration.
3. Cannot leverage the existing indoor illumination infrastructure nor provide lightning for that matter.

In conclusion, compared to Firefly, the chosen ground truth system is costly and impractical for drone positioning in a large scale applications. However, it is an effective research tool to benchmark the performance of Firefly and SoA methods.

5.3 Software implementation

In our testbed, the drone executes a flight route using the ground truth system as a reference. To move from one position to the other, the Crazyflie needs to receive a position setpoint from a remote client. This remote client is executing a python script that sends a new position setpoint every time step based on a pre-programmed route. With this information, the Crazyflie can execute a flight trajectory where it collects sensor data in real-time. Finally, the data log is sent to the remote client and then to Matlab for processing. The flow of information described above is depicted in Fig. 5.6 and the variables are clarified in the following subsections.

The main software components of our system involve the UAV, the remote client and Matlab; which we explain hereafter. Although Firefly can run in real time in the UAV, in order to visualize and provide statistical measurements of the trajectory we use Matlab as a tool. In addition, it allows us to compare the performance of different methods in Chapter 6.

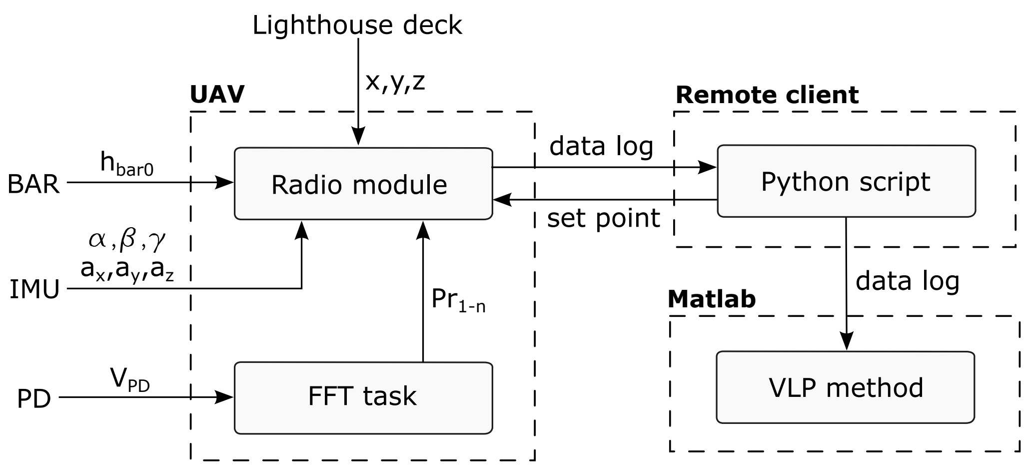

Figure 5.6: Data flow between software systems.

5.3.1 UAV

The PD is connected to a 12-bit analog to digital converter of the Crazyflie. We retrieve its measurements by creating a FreeRTOS task next to the existing firmware, which is also based on FreeRTOS tasks. When our task executes, 64 samples are obtained at a sampling frequency f_s of 1kHz. We rescale each sample from the ADC and convert it to a power measurement according to the configuration displayed in Fig. 5.4b, which results in the following linear equation:

$$P_r = \frac{V_{PD} - 0.0001}{0.045} \quad [\mu\text{W}] \tag{5.2}$$

where

$$V_{PD} = \frac{ADC \cdot V_{ref}}{2^{resolution}} = \frac{ADC \cdot 3V}{2^{12}} \tag{5.3}$$

We use the 64 samples of the received power P_r to compute the FFT of the signal and retrieve the RSS value from each individual LED. For this purpose, the ARM's CMSIS DSP library is used to compute the FFT and other dedicated operations. The CMSIS DSP library contains signal processing functions that are readily available and allow to simplify the deployment of embedded applications. Using the CMSIS DSP library it is possible to execute a 64 point FFT on the available STM32F4 processor under 25μs [36], which allows for a real-time deployment. After performing the FFT, the RSS from each transmitter is retrieved by obtaining the maximum value within a search window close to the frequency ID. For example, the RSS value for a transmitter with a frequency ID of 60 HZ will be found by searching the peak value in the window between 50 Hz and 70 Hz.

Finally, the internal data of the barometer, IMU and received power is directly transmitted to the remote client through the available radio module via the 2.4 GHz band.

5.3.2 Remote client

The remote client executes a python script which connects to the Crazyflie via radio. The python script sends position commands to the drone as time progresses so that it can follow a pre-programmed route. In addition, the python script also defines the *log configuration* of the Crazyflie, which indicates the logging rate and the variables that are sent from the drone to the client. In Table 5.2 we show the log configuration that was implemented.
From Table 5.2, we see that the transmitted variables have different logging rates. This is because the FFT consumes 64 ms for sampling (not execution) and for this reason we decide to obtain a VLP estimate just once every 100 ms. In the case of the IMU, the accelerometer data can be trusted in the *short term* as discussed in Section 4.3, and thus it is useful to update the height estimation at a faster rate using this data. The orientation, barometer and ground truth variables are still sent as fast as possible, every 20 ms, without overloading the transmitting capacity of the Crazyflie.

5.3.3 Matlab

As a final step in the software implementation, the data log obtained in the remote client is exported to Matlab, where Firefly is evaluated. To effectively use the sensor data we obtained in the real flight tests, we pre-process the digital signals in the following manner:

Source	Variable (s)	Units	Logging rate	Description
PD	$Pr1-4$	[μW]	10 Hz	Power received
IMU	a_x, a_y, a_z	[Gs]	50 Hz	Linear acceleration
	α, β, γ	[°]	20 Hz	Orientation (roll, pitch yaw)
Barometer	h_{bar0}	[m]	20 Hz	Altitude above sea level
Lighthouse deck	x, y, z	[m]	20 Hz	Ground truth position

Table 5.2: Logging rate of variables transmitted to the remote client.

- The barometer measurement is calibrated to 0 m. For example, if the first value of the barometer indicates 46.2 m (above sea level) at ground level, this is the new reference of our system.
- A low-pass filter is applied to the accelerometer to remove high frequency noise.
- A low-pass filter is applied to the received power signal to remove high frequency noise.
- We compute the mean value of the accelerometer at rest for the 2 s before lift off. The mean value of the accelerometer in each direction (a_x, a_y, a_z) is considered the constant sensor bias and is subtracted to subsequent accelerometer values to mitigate biased measurements and reduce accelerometer drift.

In order to use the value of the accelerometer, a rotation matrix must be applied to transform the acceleration in the body frame of the drone ($a_{x,y,z}$) to the reference frame (a_{ref}) using the roll, pitch and yaw (γ, β and α respectively) data, which is also obtained from the IMU. This can be done during the execution of our method. In our case, the rotation matrix follows the East, North, Up (ENU) convention of clockwise (CW) and counter-clockwise (CCW) rotations as it is the one used by the Crazyflie:

$$a_{ref} = R^{ENU} \cdot a_{x,y,z} \tag{5.4}$$

where

$$R^{ENU} = R_{\alpha}^{CW} \cdot R_{\beta}^{CCW} \cdot R_{\gamma}^{CW} \tag{5.5}$$

We use the resulting acceleration on the vertical axis of the reference frame as one of the inputs for the complementary filter.

After the sensor measurements have been pre-processed, we implement our proposed method in Matlab as described in Section 4.3.

6 EXPERIMENTAL VALIDATION

In this chapter, we evaluate Firefly and compare it with SoA methods in an indoor testbed shown in Fig. 5.1. We select two methods as reference: the *3D VLP with RSS* method in [28] and the *2D+H VLP with RSS* method in [12] which have reported favorable results, with errors below 10 cm, as previously shown in Fig. 3.4. Two metrics are used for comparison: 1) the location error, calculated as the Euclidean distance from ground truth to the output of each method, and 2) the algorithm complexity.

In Appendix A, we describe the working principles and implementation of the other methods used for comparison according to our notation and test setup. In Appendix B we also provide the project repository where the software components used to perform the tests and obtain the results presented in this thesis are available. In addition, we include a demo video to show the drone in motion during a flight test.

6.1 Setup

We carry out 8 automated flight tests to cover a circular path of radius 0.5 m and a range of heights from 0.25 m to 1.8 m. In the circular route the LEDs are always within the field of view of the PD (i.e. $\theta < \Theta_c$). In addition, when the drone is close to a direct LOS to an LED, the distance is more than 0.5 m to avoid saturation of the PD as shown in Fig. 6.1.

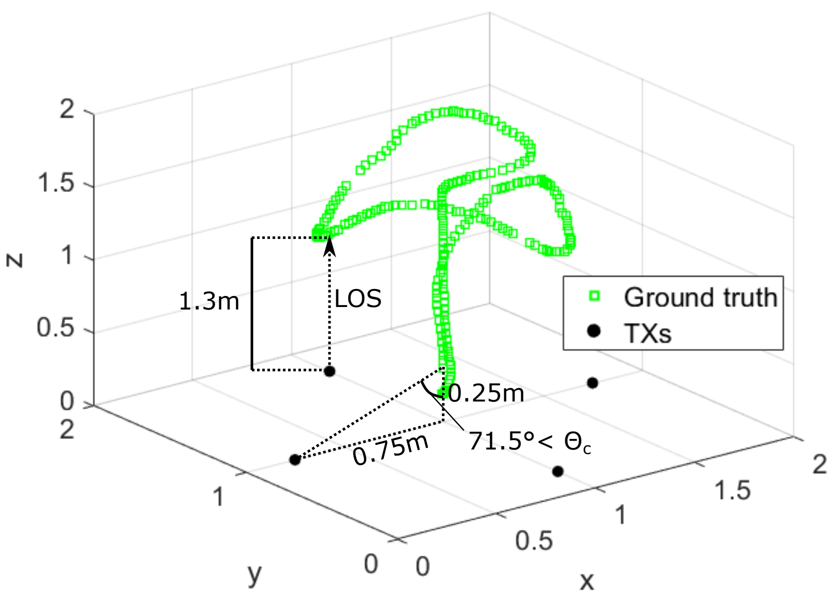

Figure 6.1: Trajectory of the drone during flight tests.

In each flight test, the drone follows the pre-programmed route from Fig. 6.1 with curves and direction changes. As a result, we are constantly inducing tilting on the drone to test the VLP methods in a real flight scenario. Along the trajectory, the drone is sampling the visible light signal and executes the FFT in real time to retrieve the ID and the RSS from each LED source.

Although Firefly can run in real time in the drone, executing the three algorithms simultaneously is too demanding. Therefore, we send the sensor data log to a remote server as previously shown in Fig. 5.1b and use Matlab to compare them. The data transmitted from the drone is listed in Table 5.2 from Chapter 5.

6.2 Positioning error

Fig. 6.2 shows the mean-error of three methods across the 8 different tests. We label the method from [12] as *Indirect-H* and the method from [28] as *3D PSO*. Firefly clearly outperforms the other two algorithms, in terms of the mean and maximum error achieved for all tests, by almost a factor of $\times 2$ and $\times 5$ with respect to Indirect-H and 3D PSO, respectively. Firefly and Indirect-H are closer in terms of accuracy compared to 3D PSO which evidently displays the lowest performance of all.

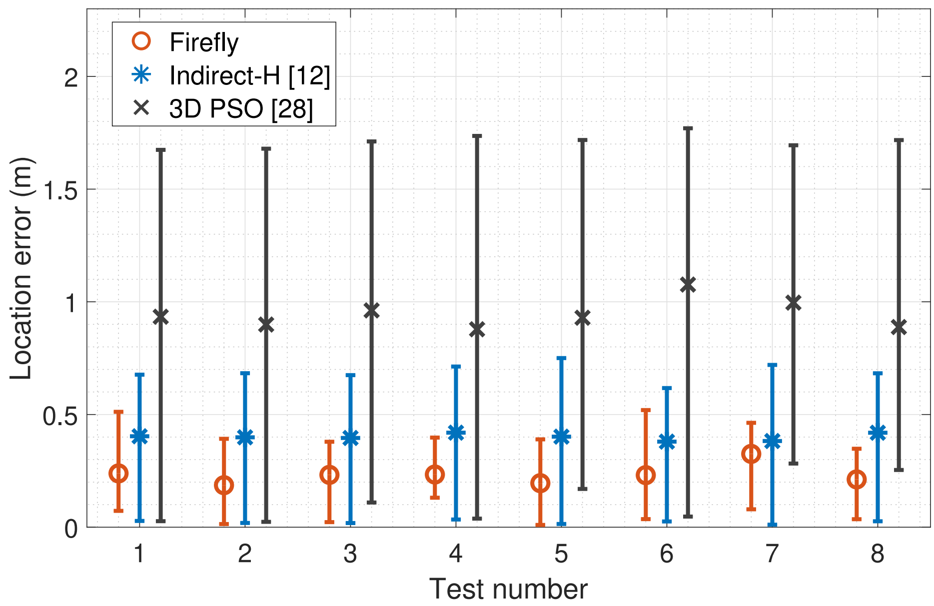

Figure 6.2: Mean-error plot for the 8 test flights.

Notice that in Fig. 3.4, in Chapter 3, the results reported by Indirect-H and 3D PSO are below 0.1 m when tested in a parallel and static scenario. However, the performance of both methods reduces significantly when tested in a mobile scenario with 6 DoF, obtaining errors around 0.4 m and 0.9 m, respectively. In Fig. 6.3 we show the results of the Indirect-H and 3D PSO next to Firefly taking into account the LED density of our test setup. We will now discuss in detail the results obtained in Firefly with respect to each method.

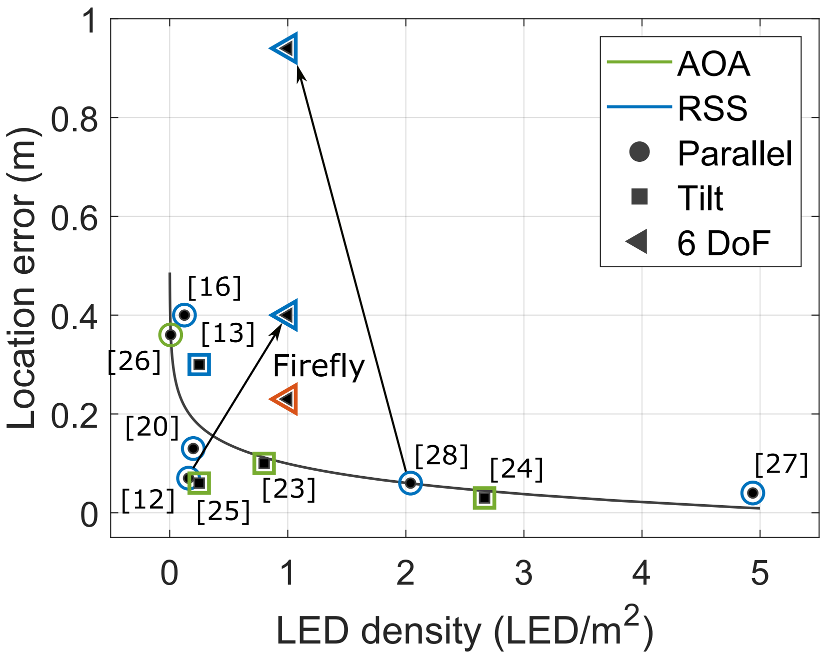

Figure 6.3: Accuracy vs LED density for different SoA studies. The curve represents the average trend of SoA studies.

6.2.1 Firefly vs. Indirect-H

Firefly Vs. Indirect-H: Let us take a close look of the Indirect-H results in one of the tests. In Fig. 6.4, we show the height estimation of Indirect-H and Firefly, and the receiver angles during the flight test. During the lift-off (timestep 0 to 60) and landing (after timestep 200), Indirect-H is able to detect the monotonic changes in altitude, but to a much smaller extend compared to Firefly. More significantly, during the route (timestep 60 to 200), Indirect-H fails to capture the variation in the height. In contrast, Firefly closely resembles the profile of the ground truth, and does not show any significant drift effect over the whole flight test.

Considering the measurements of all tests, the mean absolute height error for Firefly is less than 14 cm compared to a mean error of 30 cm of the Indirect-H method. In our tests, the drone is exposed to tilting angles up to 7° as shown in Fig. 6.4 (bottom). Although *some* of the errors of the Indirect-H method can be attributed to tilting, the height estimation does not accurately reflect the ground truth even when the tilting angle of the receiver is small. For example, in the segment between timestep 100 and 150, the roll and pitch angles are less than 2°. Even though the receiver and transmitter are close to parallel during this time, we can see that the estimated height by the Indirect-H method does not match to the ground truth from Fig. 6.4 (top). The error in the Indirect-H method can be further explained due to speed variations and vibrations particular of a mobile environment, and sensitivity of the method to parameters not considered in their model, such as optical gain of the receiver. Our approach considers the input of the indirect method but only with a small weight ϵ to compensate drifts, c.f. Fig. 4.4. As a result, Firefly produces an accurate height estimation using multi-sensor fusion.

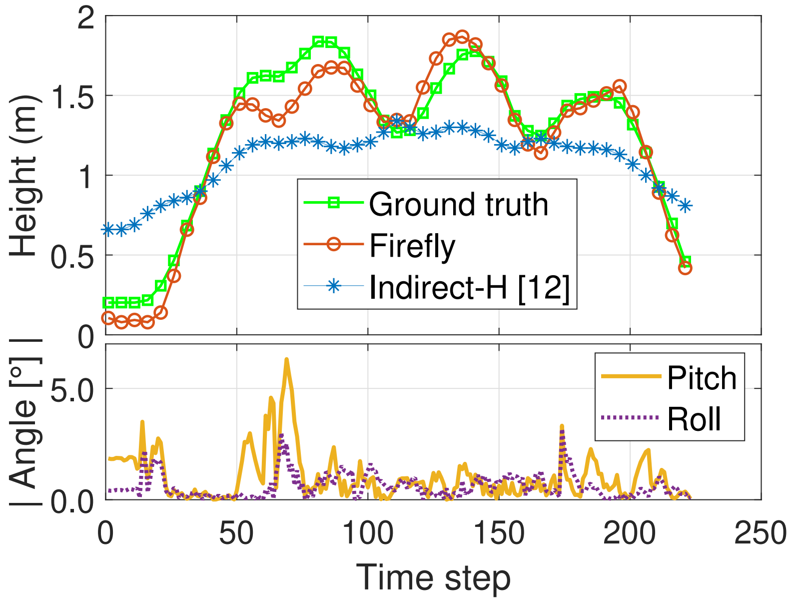

Figure 6.4: Height estimation (top) and tilting angles of the receiver (bottom) in Test 5.

In Fig. 6.5b, we now analyze the 2D position by looking at the top view of the trajectory for the same test. The Indirect-H estimation roughly captures the circular motion of the actual drone, but not with the amplitude seen in the ground truth. Firefly achieves a wider amplitude in the x-y plane that is closer to ground truth. Since the 2D position of the receiver is computed with the same RSS information in both methods, this improvement of the 2D position can be mainly attributed to (1) an accurate height estimation using a sensor-fusion approach and (2) the consideration of tilting of the receiver into the equations.

Fig. 6.5a depicts the 3D trajectory of both methods. It supports our previous analysis that Firefly provides a more accurate location than Indirect-H. From the statistical measurements of the position error of all 8 tests, Firefly improves the accuracy by around 42% as listed in Table 6.1.

	Indirect-H [12]	**Firefly**	**Improvement**
Mean error (cm)	40.01	23.19	42.05%
Median error (cm)	41.02	23.62	42.41%
Max. error (cm)	68.98	42.52	38.35%
Std. dev. (cm)	15.68	9.64	38.53%

Table 6.1: Improvement of positioning accuracy.

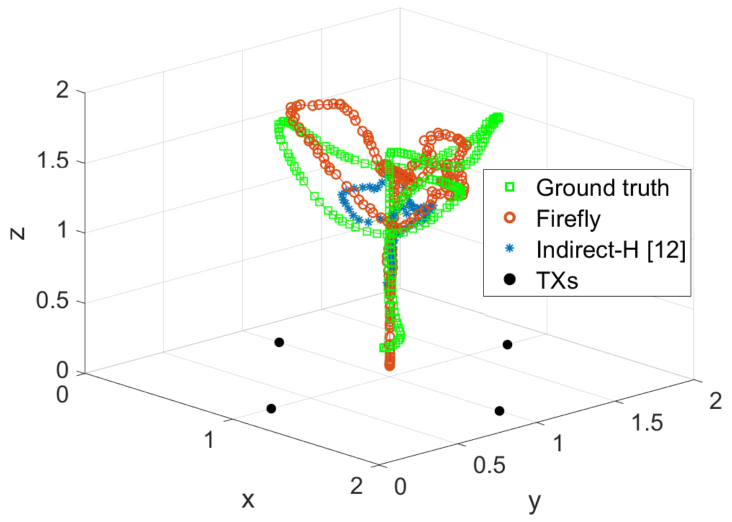

(a) 3D Trajectory

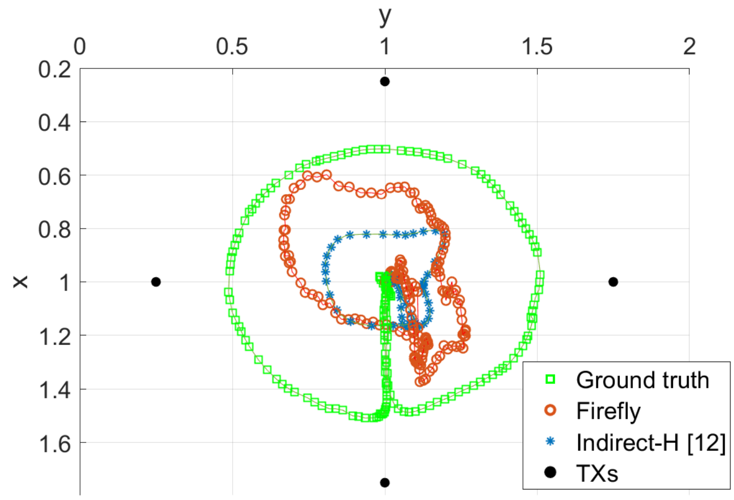

(b) 3D Trajectory (Top View)

Figure 6.5: Firefly vs. Indirect-H [12] in Test 5.

6.2.2 Firefly Vs. 3D PSO

Firefly Vs. 3D PSO: In another test example, shown in Fig. 6.6a, we look into the estimated trajectory of the 3D PSO method. 3D PSO displays the expected circular motion in the x-y plane, but the altitude estimation is far from the ground truth, and up to the imposed upper bound of the test area (i.e. 2 m). In Fig. 6.6b, the top view of the trajectory for the same test is shown and we see that the amplitude of the trajectory is very wide compared compared to the ground truth. 3D PSO does not perform as well as the other methods and has a mean positioning error of 94.54 cm.

The inaccurate results of 3D PSO can be explained because its model considers parallel transmitters and receiver. In the method, the gain of the system (i.e. ratio of the received and transmitted power) is used to estimate the x, y, z coordinates that most accurately describe the channel loss (similar to Eq. (2.3)). However, the channel loss cannot be obtained from the power received directly because the distance is also affected by the height of the receiver. When the assumptions of the model are broken, small angle variations can have a significant effect in the distance calculation as the height is not known. Thus, the 3D position cannot be determined precisely.

In our test, we show that 3D RSS methods are not effective strategies to determine the position of UAVs. Although they have provided favorable results when tested under controlled conditions, when tilting and movement are introduced, the position accuracy is severely downgraded.

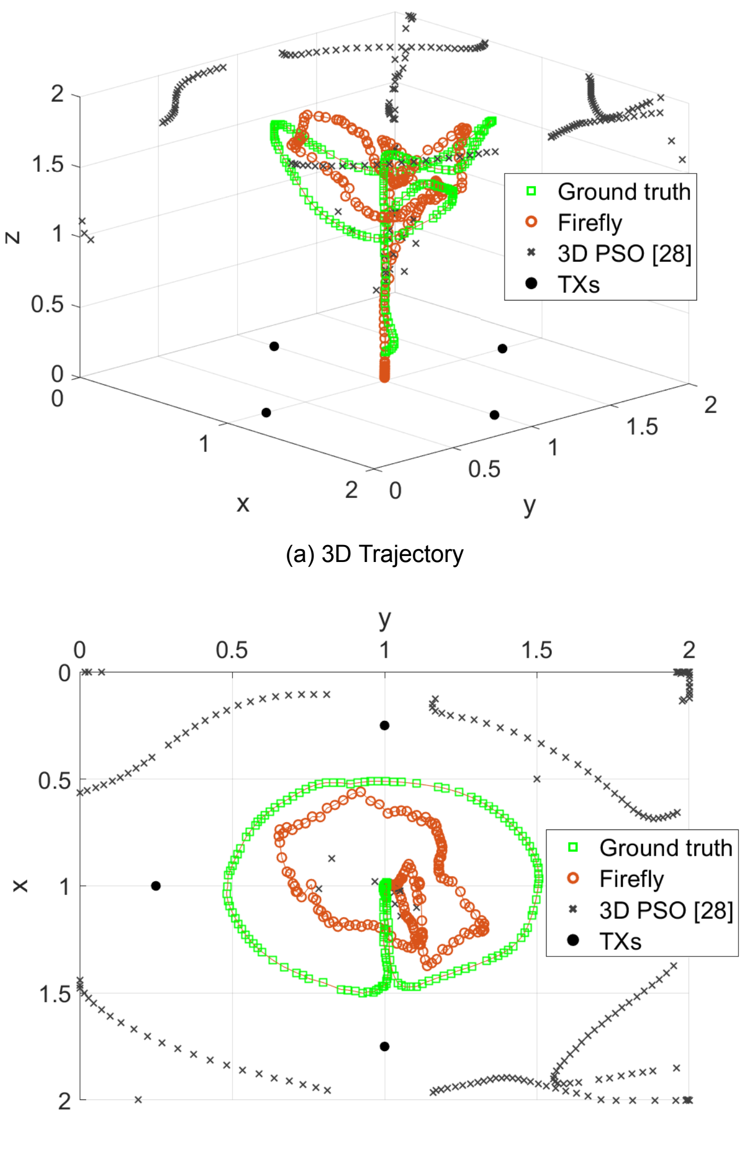

(b) 3D Trajectory (Top View)

Figure 6.6: Firefly vs. 3D PSO [28] in Test 8.

6.3 Algorithmic complexity

The 3D PSO method considers multiple particles (candidate solutions) that are evaluated at each iteration. This results in multiple function evaluations and a quadratic complexity $O(n^2)$ without taking into account additional modifications of the method. In [27] and [28], 20 iterations of the method are allowed and a particle group size of 200 is considered in the latter study which results in up to 4000 function evaluations.

In the Indirect-H method, the height is computed by iteratively evaluating a set of candidate heights in the range of interest. To evaluate each candidate solution, a trilateration step is performed for each height candidate. Considering the proposed resolution of 1 mm and the height of our setup (2 m), this would amount to 2000 evaluations. The time complexity of this iterative approach is $O(n)$ if we consider that the computation time of each iteration (consisting of a trilateration step) is constant. A fast search optimization of the algorithm is also proposed in [12] to narrow the search interval. This reduces the computation time by 90% and the time complexity improves to $O(\log(n))$.

In Firefly, we implement the complementary filter proposed in [31] to estimate the height, which consists of two discrete equations that can be computed in one step respectively. Then, we execute a 2D trilateration method twice. Considering the computation time of the trilateration steps constant (as we do for the Indirect-H method), the time complexity of the previous steps is $(O(1))$. When we apply the long term drift correction for the barometer, we also use the Indirect-H method to remove zero drift. Therefore, our algorithm has a time complexity of $O(\log(n))$ considering an implementation of the fast search algorithm of Indirect-H. However, in our empirical evaluations, we find that the barometer correction can be executed less frequently without a considerable impact on the positioning accuracy. This results in a time complexity of $O(\log(n/k))$, where k indicates that the barometer correction is executed once for every k iterations of our method. When $k = 10$, we find that the mean error of Firefly only increases by 1.6 cm.

6.4 Limitations of Firefly

We have seen the benefits of using sensor data to directly estimate height and orientation compared to the Indirect-H approach. Even in the worst performing flight test of Firefly (in test 7), the positioning error is lower that in the best results obtained for Indirect-H and 3D PSO. However, Firefly still has some limitations that will be discussed hereafter, and can serve as the basis for future work.

In Fig. 6.7, the height of Firefly observed in test 7 resembles the altitude profile of the ground truth, but it moderately *drifts* down from the actual position. We have identified this potential problem in barometers in Section 4.3.2, which can be explained due to temperature or pressure changes in the room, or temporary wind drafts. These variables did not have a noticeable effect during our flight tests, except in test 7, which suggest that they can occur occasionally. To mitigate the influence of wind drafts, the barometer can be isolated from the rest of the environment with a cover. To prevent zero-drift from temperature and pressure changes in the room, we proposed the drift correction scheme shown in Fig. 4.4, which will prevent major error drift over a larger time window. To further remove the effects of barometer drift, different alternatives for corrections can be explored. For instance, using the measurements of the Indirect-H method where it provides accurate location results, e.g., in strictly static and parallel situations, but avoiding forced stops that would impact the trajectory of the drone.

The height estimation can also be further improved from the IMU measurements. In Section 5.3.3 we mentioned that a constant bias is considered when using the accelerometer readings. The constant sensor bias is obtained during a two second period where the drone is at rest, and improves the performance of the method since sensor bias is compensated. However, accelerometer bias will change too over time, and for this reason we can only trust the accelerometer in the short term and we use the barometer for long term reference. If the accelerometer bias is estimated on-line, the sensor can be trusted for longer periods of time leading to a more accurate altitude estimation for the UAV. Online bias estimation has been demonstrated with positive results, for example in [37], but further analysis is required to evaluate the cost-effectiveness of the solution taking into account the added complexity.

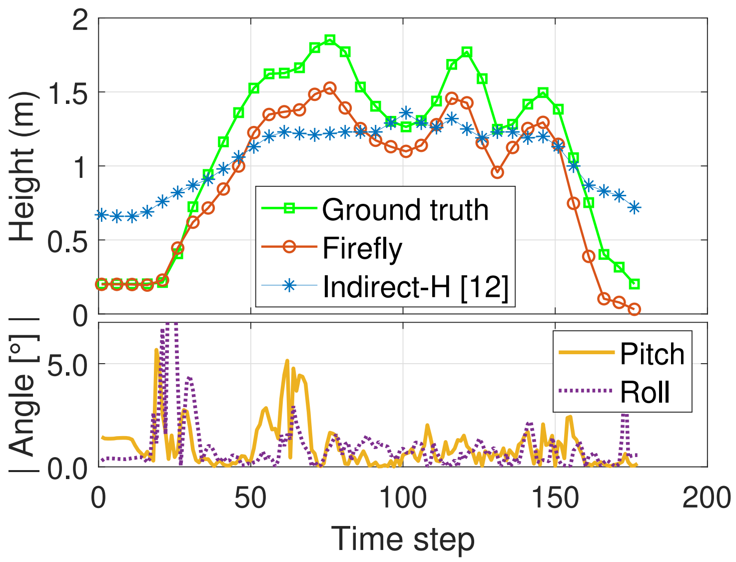

Figure 6.7: Height estimation (top) and tilting angles of the receiver (bottom) in Test 7.

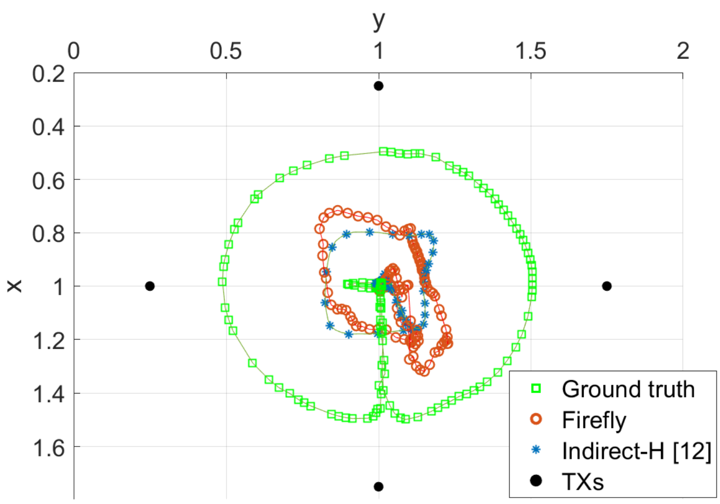

Figure 6.8: Firefly vs. Indirect-H [12] in Test 7.

Considering now the 2D position for test 7, in figure Fig. 6.8 we show the top view of the flight trajectory. It can be seen that when the height estimation is not as accurate, the 2D position is also affected (as in the case of Indirect-H). In our tests, we observed that when the height estimation is above ground truth, the amplitude of the 2D trajectory tends to expand, and when the height is below ground truth, the amplitude tends to shrink (as in Test 7). This is consistent with Eq. (4.3), which indicates that when the height estimation decreases, the distance does too, and vice versa. Although Firefly provides a more accurate altitude estimation than Indirect-H, it would still benefit the 2D estimation to be more resilient to height errors. One possibility to overcome the limitations of the 2D position, is to use the values of the accelerometer in the x-y plane to improve the positioning accuracy.

7 CONCLUSION

This work illustrates, for the first time, that VLC can be used for accurate 3D positioning for drones with six degrees of freedom in a realistic experimental setup. It paves the way for using standard light bulbs to provide navigation services for drones. A novel localization method, Firefly, is proposed by building upon the line of research that decomposes a 3D positioning problem into 2D+H. Compared to SoA studies, it removes the need of imposing complex requirements on the transmitter and receiver designs to achieve an accurate positioning result. In addition, it overcomes the limitation of the SoA RSS methods, which are restricted to parallel receiver and transmitters without considering tilting. By utilizing on-board sensors on the drone, we accurately estimate height and account for tilting of the receiver. The algorithm is also lightweight and can be implemented in a drone for real-time execution. As demonstrated by the experimental results, Firefly achieves mean position accuracy of 23.19 cm using off-the-shelf LED lights and low-cost sensors. It reduces the localization error compared to other SoA methods by around 42% under the same experimental setup.

7.1 Future work

To continue this work, some opportunities were mentioned when discussing the limitations of Firefly in Section 6.4. The long term drift correction scheme for the barometer could be enhanced to exploit the favorable properties of the Indirect-H method when the drone is static. The accelerometer bias could be estimated during flight to provide more reliable measurements of acceleration that would result in higher accuracy of the method. The 2D position estimation could be potentially improved utilizing accelerometer data. In addition, the wireless optical channel we considered in Eq. (2.4) can be augmented to consider other parameters of a non-ideal environment including noise and optical gain of the receiver, which varies depending on the incidence angle. In relation with non-ideal environments, the framework of Firefly can be enhanced to be robust against ill-conditioned scenarios and multipath effects as discussed in Table 2.1. Finally, more extensive tests, including longer time frames and different flight routes will provide more information about the challenges of VLP with UAVs, and provide new research paths on how to address them.

REFERENCES

[1] P. H. Pathak, X. Feng, P. Hu, and P. Mohapatra. Visible light communication, networking, and sensing: A survey, potential and challenges. *IEEE Communications Surveys Tutorials*, 17(4):2047–2077, 2015.

[2] P. Kuppusamy, S. Muthuraj, and S. Gopinath. Survey and challenges of Li-Fi with comparison of Wi-Fi. In *2016 International Conference on Wireless Communications, Signal Processing and Networking (WiSPNET)*, pages 896–899, 2016.

[3] Mohammed M. A. Mohammed, Cuiwei He, Stefanie Cincotta, Adrian Neild, and Jean Armstrong. Communication aspects of visible light positioning (VLP) systems using a quadrature angular diversity aperture (QADA) receiver. *Sensors*, 20(7), 2020.

[4] Milad Afzalan and Farrokh Jazizadeh. Indoor positioning based on visible light communication: A performance-based survey of real-world prototypes. *ACM Comput. Surv.*, 52(2), May 2019.

[5] Yousef Almadani, Muhammad Ijaz, Sujan Rajbhandari, Bamidele Adebisi, and Umar Raza. Application of visible light communication in an industrial environment. In *2018 11th International Symposium on Communication Systems, Networks Digital Signal Processing (CSNDSP)*, pages 1–6, 2018.

[6] Yousef Almadani, Muhammad Ijaz, Sujan Rajbhandari, Umar Raza, and Bamidele Adebisi. Dead-zones limitation in visible light positioning systems for unmanned aerial vehicles. In *2019 Eleventh International Conference on Ubiquitous and Future Networks (ICUFN)*, pages 419–421. IEEE, 2019.

[7] Eyesee. (2021). [Online]. Available: https://eyesee-drone.com/.

[8] DroneScan. (2021). [Online]. Available: https://www.dronescan.co/.

[9] Tyler Duvall, Alastair Green, Langstaff Meredith, and Kayla Miele. Air-mobility solutions: What they'll need to take off. McKinsey, Feb. 2019.

[10] Trong-Hop Do and Myungsik Yoo. An in-depth survey of visible light communication based positioning systems. *Sensors*, 16(5), 2016.

[11] Y. Zhuang, L. Hua, L. Qi, J. Yang, P. Cao, Y. Cao, Y. Wu, J. Thompson, and H. Haas. A survey of positioning systems using visible led lights. *IEEE Communications Surveys Tutorials*, 20(3):1963–1988, 2018.

[12] David Plets, Yousef Almadani, Sander Bastiaens, Muhammad Ijaz, Luc Martens, and Wout Joseph. Efficient 3D trilateration algorithm for visible light positioning. *Journal of Optics*, 21(5):05LT01, Apr. 2019.

[13] Yousef Almadani, Muhammad Ijaz, Wout Joseph, Sander Bastiaens, Sujan Rajbhandari, Bamidele Adebisi, and David Plets. A novel 3D visible light positioning method using received signal strength for industrial applications. *Electronics*, 8(11), 2019.

[14] United states department of energy. energy savings forecast of solid-state lighting in general illumination applications. (Mar. 2021). [Online]. Available: http://apps1.eere.energy.gov/buildings/publications/pdfs/ssl/energysavingsforecast14.pdf.

[15] Official U.S. government information about the global positioning system (GPS) and related topics. (Mar. 2021). [Online]. Available: https://www.gps.gov/systems/gps/performance/accuracy/.

[16] Liqun Li, Pan Hu, Chunyi Peng, Guobin Shen, and Feng Zhao. Epsilon: A visible light based positioning system. In *11th USENIX Symposium on Networked Systems Design and Implementation (NSDI 14)*, pages 331–343, 2014.

[17] Mohamed A Dawood, Sally S Saleh, El-Sayed A El-Badawy, and Moustafa H Aly. A comparative analysis of localization algorithms for visible light communication. *Optical and Quantum Electronics*, 53(2):1–25, 2021.

[18] N. Nguyen, N. Nguyen, V. Nguyen, K. Sripimanwat, and A. Suebsomran. Improvement of the VLC localization method using the extended kalman filter. In *TENCON 2014 - 2014 IEEE Region 10 Conference*, pages 1–6, 2014.

[19] Ashwin Ashok. Position: Dronevlc: Visible light communication for aerial vehicular networking. In *Proceedings of the 4th ACM Workshop on Visible Light Communication Systems*, VLCS '17, page 29–30, New York, NY, USA, 2017. Association for Computing Machinery.

[20] Y. Zhuang, L. Hua, Q. Wang, Y. Cao, Z. Gao, L. Qi, J. Yang, and J. Thompson. Visible light positioning and navigation using noise measurement and mitigation. *IEEE Transactions on Vehicular Technology*, 68(11):11094–11106, 2019.

[21] Wenjun Gu, Mohammadreza Aminikashani, Peng Deng, and Mohsen Kavehrad. Impact of multipath reflections on the performance of indoor visible light positioning systems. *Journal of Lightwave Technology*, 34(10):2578–2587, 2016.

[22] Y. S. Eroglu, F. Erden, and I. Guvenc. Adaptive kalman tracking for indoor visible light positioning. In *MILCOM 2019 - 2019 IEEE Military Communications Conference (MILCOM)*, pages 331–336, 2019.

[23] A. Şahin, Y. S. Eroğlu, İ. Güvenç, N. Pala, and M. Yüksel. Hybrid 3-D localization for visible light communication systems. *Journal of Lightwave Technology*, 33(22):4589–4599, 2015.

[24] B. Zhu, J. Cheng, Y. Wang, J. Yan, and J. Wang. Three-dimensional VLC positioning based on angle difference of arrival with arbitrary tilting angle of receiver. *IEEE Journal on Selected Areas in Communications*, 36(1):8–22, 2018.

[25] Se-Hoon Yang, Hyun-Seung Kim, Yong-Hwan Son, and Sang-Kook Han. Three-dimensional visible light indoor localization using AOA and RSS with multiple optical receivers. *Journal of Lightwave Technology*, 32(14):2480–2485, 2014.

[26] Bo Xie, Kongyang Chen, Guang Tan, Mingming Lu, Yunhuai Liu, Jie Wu, and Tian He. Lips: A light intensity–based positioning system for indoor environments. *ACM Transactions on Sensor Networks (TOSN)*, 12(4):1–27, 2016.

[27] Y. Cai, W. Guan, Y. Wu, C. Xie, Y. Chen, and L. Fang. Indoor high precision three-dimensional positioning system based on visible light communication using particle swarm optimization. *IEEE Photonics Journal*, 9(6):1–20, 2017.

[28] C. Carreño, F. Seguel, P. Adasme, I. Soto, N. Krommenacker, P. Charpentier, and V. Bombardier. Comparison of metaheuristic optimization algorithms for RSS-based 3-D visible light positioning systems. In *2020 South American Colloquium on Visible Light Communications (SACVC)*, pages 1–6, 2020.

[29] Steven De Lausnay, Lieven De Strycker, Jean-Pierre Goemaere, Nobby Stevens, and Bart Nauwelaers. A visible light positioning system using frequency division multiple access with square waves. In *2015 9th International Conference on Signal Processing and Communication Systems (ICSPCS)*, pages 1–7, 2015.

[30] Oliver J Woodman. An introduction to inertial navigation. Technical report, University of Cambridge, Computer Laboratory, 2007.

[31] Walter T. Higgins. A comparison of complementary and kalman filtering. *IEEE Transactions on Aerospace and Electronic Systems*, AES-11(3):321–325, 1975.

[32] Angelo Maria Sabatini and Vincenzo Genovese. A sensor fusion method for tracking vertical velocity and height based on inertial and barometric altimeter measurements. *Sensors*, 14(8):13324–13347, 2014.

[33] Luchi Hua, Yuan Zhuang, Longning Qi, Jun Yang, and Longxing Shi. Noise analysis and modeling in visible light communication using allan variance. *IEEE Access*, 6, 2018.

[34] Emanuele Goldoni, Alberto Savioli, Marco Risi, and Paolo Gamba. Experimental analysis of RSSI-based indoor localization with ieee 802.15.4. pages 71 – 77, 05 2010.

[35] Qing Wang, Domenico Giustiniano, and Daniele Puccinelli. OpenVLC: Software-defined visible light embedded networks. In *Proceedings of the 1st ACM MobiCom workshop on Visible light communication systems*, pages 15–20, 2014.

[36] ST Microelectronics. Digital signal processing for STM32 microcontrollers using CMSIS. (Ago. 2021). [Online]. Available:
https://www.st.com/resource/en/application_note/dm00273990-digital-signal-processing-for-stm32-microcontrollers-using-cmsis-stmicroelectronics.pdf.

[37] Youngbin Son and Seyoung Oh. A barometer-IMU fusion method for vertical velocity and height estimation. In *2015 IEEE SENSORS*, pages 1–4, 2015.

A APPENDIX A. SOA METHODS USED FOR COMPARISON

A.1 Indirect-H

The *2D+H* method from [12] that we use as comparison for Firefly minimizes the following cost function. The approach considers the difference between the distance for a given (assumed) candidate height, and the calculated distance for the same height after 2D trilateration:

$$
\begin{aligned}
\underset{h}{\text{minimize}} \quad & C(h) = \frac{1}{N}\sum_{i=1}^{N}\left(d_i(h) - \sqrt{(x_r(h)-x_i)^2 + (y_r(h)-y_i)^2 + (h-z_i)^2}\right)^2 \\
\text{subject to} \quad & h \succeq 0 \\
& h \preceq 2 \text{ (height of our testbed in [m])}
\end{aligned}
\tag{A.1}
$$

This approach allows to obtain the most likely height given a 2D trilateration result. The distance $d_i(h)$ to each i anchor point is obtained using Eq. (4.3), which assumes that the transmitter and receiver are parallel. The final position is obtained with the following procedure:

Algorithm 1 Iterative Indirect-H method.

Require: $N \geq 3$ (N anchor points)

for $h = 0 : h_{step} : h = 2$ **do**

1. Calculate the distance $d_i(h)$ to each i anchor point with Eq. (4.3)
2. Calculate x_r, y_r with 2D trilateration using $d_i(h)$ (similarly to Section 4.3.2)
3. Obtain the cost $C(h)$ from Eq. (A.1)

end for

Select the h and corresponding x_r, y_r that minimizes C(h) from Eq. (A.1)

By iterating over the range of height values, with a resolution of $h_{step} = 0.01m$ we obtain the 3D position as a result of a *2D+H* procedure.

A.2 3D PSO

The *3D VLP with RSS* method from [28] attempts to minimize the error of the following cost function by finding the position that reduces the difference between the estimated and obtained channel gain:

$$\begin{aligned} \underset{x_r, y_r, z_r}{\text{minimize}} \quad & \sum_{i=1}^{N} \left(H_i^{LOS} - \frac{P_{r,i}}{P_{t,i}} \right)^2 \\ \text{subject to} \quad & (x_r, y_r, z_r) \succeq 0 \\ & (x_r, y_r, z_r) \preceq (2, 2, 2) \;\; \text{(size of our testbed in [m])} \end{aligned} \tag{A.2}$$

The channel gain H_i^{LOS} is similar to Eq. (2.3), but includes the parallel assumption from Eq. (4.2) and does not consider tilting. The distance to the *i*-th anchor point is calculated with the candidate position estimates from the PSO algorithm as the euclidean distance:

$$d_{i,PSO} = \sqrt{(x_i - x_r)^2 + (y_i - y_r)^2 + (z_i - z_r)^2} \tag{A.3}$$

The position estimation x_r, y_r, z_r that minimizes Eq. (A.2) is selected according to the stop criteria of the PSO algorithm. Here we consider 20 iterations as in the original study.

B APPENDIX B. PROJECT REPOSITORY

The necessary components to replicate the results presented in this thesis are contained in the following project repository:

`https://github.com/rampudia15/portfolio/tree/master/VLP_UAVs/`

The **FreeRTOS task** that was added to the Crazyflie firmware to interface with the PD deck is found here:
`https://github.com/rampudia15/portfolio/tree/master/VLP_UAVs/C`

The **Python script** used to control the trajectory of the drone in the remote client is available in:
`https://github.com/rampudia15/portfolio/tree/master/VLP_UAVs/Python`

The **Matlab program** used to process the data from real flight tests is available here:
`https://github.com/rampudia15/portfolio/tree/master/VLP_UAVs/Matlab`

VLP_method_comparison.m produces the 2D and 3D plots of a selected test and *VLP_method_comparison_stats.m* computes the statistics for all 8 tests available.
No additional configuration is needed to run the scripts, although the installation of the *Global Optimization Toolbox* in Matlab is required.

A **demo video** of the testbed during a flight test is found here:
`https://github.com/rampudia15/portfolio/tree/master/VLP_UAVs/demo_video`